Author's accepted manuscript. The published version of record is: Yao, X., Kim, M., Dronova, I., McBride, J. R., Kondolf, G. M., & Radke, J. D. (2025). *Landscape and Urban Planning*, 263, 105420. https://doi.org/10.1016/j.landurbplan.2025.105420.
© 2025 The Authors. Distributed under a CC BY 4.0 license.

Highlights

Community-scale microclimate simulation using Airborne Laser Scanning and object-based urban tree classification

Xihan Yao, Minho Kim, Iryna Dronova, Joe R. McBride, G. Mathias Kondolf, John D. Radke

- Lidar-based urban tree classification is integrated with microclimate simulation.
- Lidar-derived metrics enable accurate urban tree family and size classification.
- Urban forests' composition differences influence cooling effectiveness.
- Wealthier communities see greater future cooling benefits from forest growth.
- The workflow provides insights for ensuring urban equity and informed planning.

Community-scale microclimate simulation using Airborne Laser Scanning and object-based urban tree classification

Xihan Yao[a,*], Minho Kim[a], Iryna Dronova[a,b], Joe R. McBride[a], G. Mathias Kondolf[a], John D. Radke[a,c]

[a]*Department of Landscape Architecture and Environmental Planning, University of California at Berkeley, Berkeley, 94720, CA, USA*
[b]*Department of Environmental Science, Policy & Management, University of California at Berkeley, Berkeley, 94720, CA, USA*
[c]*Department of City and Regional Planning, University of California at Berkeley, Berkeley, 94720, CA, USA*

Abstract

Urban climate and urban heat island effects, resulting from urban development and expansion, significantly impact human health and well-being. Urban forests play a vital role in regulating urban climate by cooling the ambient environment through shade and evapotranspiration, among many essential ecosystem services. Different human communities have distinct abundances, compositions, and patterns of urban forests, leading to varied cooling effectiveness and microclimate outcomes. While the general consensus is that planting more trees yields greater benefits, there is an increasing need to understand and document the forests' varied taxonomical, structural, and biophysical properties at a more granular scale. This understanding is crucial to predicting and comparing the consequent microclimate conditions across communities. In this study, we utilize high-density airborne point cloud data (58 pulses per m^2) to differentiate trees based on their vertical and internal structures. We create a tree family and size classification map for all trees in two socioeconomically distinct communities in Portland, Oregon, USA. The Random Forest classifier, using Lidar-derived metrics, classifies all tree objects into seven classes with an overall accuracy of 67.1%. Using

*Corresponding author.
Email address: xyaoaf@berkeley.edu (Xihan Yao)

the classified properties, we simulate and compare these forests' combined air temperature cooling effects and test alternative tree composition scenarios with the object-based ENVI-met model. The simulation results indicate that wealthier communities experience a more significant reduction in 1.5-meter-above-ground air temperature than less wealthy communities (0.23K cooler on average). This disparity in benefits is likely to widen further if current forest evolution trends persist. This study demonstrates a comprehensive workflow from generating object-based knowledge on urban trees to high spatial resolution microclimate simulation of the urban forests' composite effects. This approach can aid in practical urban forest quality monitoring and evaluation, supplement urban planning and management practices, and optimize the urban forest to facilitate cross-community ecosystem services equity.

Keywords: Airborne Laser Scanning, Urban forest, Microclimate, ENVI-met, Urban remote sensing, Ecosystem services

---

1. Introduction

Urban forests provide a range of local and micro-scale ecosystem services that benefit local human communities (Bolund & Hunhammar, 1999; Nowak & Dwyer, 2007). In particular, urban trees regulate the climate, which cools the ambient environment primarily through shading and evapotranspiration, significantly contributing to residents' health and wellbeing (Bowler et al., 2010; J. Kim et al., 2024; Wolf et al., 2020). The urban climate differs from the regional natural background climate and is highly heterogeneous across different parts of the city, influenced by various local environmental and landscape factors such as urban morphology, materials, heat emissions, and natural features (Grimmond, 2007). Such heterogeneity often means inequity, with some communities suffering from hotter air temperatures and higher associated risks compared to others in the same city (Hoffman et al., 2020). To address these disparities and mitigate emerging climate threats, cities worldwide are implementing various nature-based solutions. These include constructing buildings with radiative reflective materials (Akbari et al., 2005), introducing water features (Hathway & Sharples, 2012), and, very importantly, increasing urban vegetation by planting more trees (McPherson et al., 2011). As a result, there is a growing interest in understanding the condition of urban forests and predicting the benefits they can provide to

urban environments (Escobedo et al., 2019; Livesley et al., 2016).

Remote sensing has demonstrated great potential for studying urban forests and expanding the scope of surveys compared to field measurements, which can be expensive and often limited in terms of spatial coverage and completeness (Klobucar et al., 2021; Shahtahmassebi et al., 2021). Various studies have utilized spaceborne or airborne remote sensing products to quantify urban vegetation abundance through indices such as the Normalized Difference Vegetation Index (NDVI) (Yuan & Bauer, 2007). Many of these studies have compared temporal changes and spatial differences in vegetation indices to explain the evolution of urban forests and cross-community discrepancies (Buyantuyev & Wu, 2010; Gottesman & Shierman, 2019). These indices can be correlated with physical and social factors such as local temperature and socioeconomic background, with many studies concluding that wealthier communities often have more abundant urban vegetation and cooler climates. These findings underscore the importance of addressing these disparities by enhancing vegetation in disadvantaged communities, where remote sensing can be a valuable tool in guiding interventions. (Jenerette et al., 2011; Jesdale et al., 2013; Nesbitt & Meitner, 2016; Schwarz et al., 2015).

Traditional remote sensing methods for detecting and mapping urban vegetation typically rely on pixel-based indices, which produce continuous grids of vegetation metrics. However, these approaches may lack the spatial precision and detail necessary for effective urban forest management. There is a growing interest among professionals in understanding the species composition, structure, and conditions of urban forests (McPherson et al., 2016). Measuring and monitoring these aspects of urban forests thus become crucial for evaluating the effectiveness and efficiency of different forests' climate-regulating services, comparing cross-community inequities, and informing practical urban planning strategies for sustainable development (Steenberg et al., 2017; Yao & Kim, 2023; Zhao & Sander, 2018). Emerging studies are treating forests as clusters or individual tree objects, examining their internal structures and classifying them based on varied biophysical properties, such as different species (Gašparović et al., 2023; Roberts et al., 2015; C. Wang et al., 2023) and cooling services effectiveness (Kong et al., 2014; I. K. McRae, 2017). To achieve these goals, analyzing Airborne Laser Scanning (ALS), or Lidar (Light detection and ranging), point cloud data has become popular (Fassnacht et al., 2016). Lidar is an active remote sensing method that offers insights into the vertical and internal structure of forests (Hancock et al., 2017). Lidar has been used to delineate individual tree crowns

and taxonomically classify trees by species in natural and urban settings, revealing significant differences in ecosystem service potential (Alonzo et al., 2014; Deng et al., 2016; L. Liu et al., 2017; Michałowska & Rapiński, 2021; K. Wang et al., 2018; Yu et al., 2011; Z. Zhang et al., 2016).

Once tree-level properties are found, there are multiple ways to measure local and microclimate conditions to support the evaluation of how trees regulate ecosystem services related to the microclimate. In-situ measurements are precise and direct but are limited by the number of observations and the cost of data acquisition, often making them inadequate for large-scale studies (Shandas et al., 2019; Voelkel & Shandas, 2017). One widely used remote sensing product for urban climate parameters is the Landsat Land Surface Temperature (LST) data (Weng et al., 2004; Zhou et al., 2019), available since Landsat 5, with the current Landsat 8 & 9 satellite offering the data 100-meter resolution. This product is often utilized within studies under the Local Climate Zone (LCZ) framework, which classifies landscapes based on their morphology to support local, mesoscale urban climate studies (Jiang et al., 2021; Stewart & Oke, 2012). While LST can serve as a proxy for the air temperature that humans feel, it represents a different meteorological concept and often cannot fully indicate local climate conditions (Chakraborty et al., 2022; Naserikia et al., 2023). Moreover, the 100-meter resolution is still too coarse for urban vegetation planning and management, and the LCZ concept is too generic, emphasizing differences across various zones while neglecting potential discrepancies within areas of the same LCZ (Aslam & Rana, 2022; Chieppa et al., 2018).

To overcome the limitations of measuring and understanding the microclimate impacts of different urban landscapes, various urban climate simulation models have been developed (Jänicke et al., 2021). These models, such as SOLWEIG (Lindberg et al., 2008), PALM (Maronga et al., 2015), and ENVI-met (Bruse & Fleer, 1998), account for the physical processes of heat and material transformation. They are designed to simulate the urban climate environment at different scales and complexities, enhancing their ability to reflect varying levels of detail in different aspects of the urban environment. Among these tools, ENVI-met is one of the most popular and actively developed ones, used extensively in both scientific research and professional practice (Z. Liu et al., 2021; Tsoka et al., 2018). ENVI-met excels in high-resolution 3D microclimate simulation, and the model can specify detailed landscape materials and object-based tree models with distinct physical properties, which can significantly affect the outcome (Smithers et al., 2018).

This feature allows users to simulate and compare the effects of different tree species on the microclimate, test alternative tree planting scenarios, and suggest effective tree planting or management strategies for future services (Z. Liu et al., 2018; I. McRae et al., 2020; Yao & Kim, 2024). ENVI-met also includes a Fractal-Based Tree Digitalization method for setting up distinct tree model objects representing different tree species and sizes (Simon et al., 2020), as different types of trees may carry distinct shading or transpiration properties (Konarska et al., 2016; Rahman et al., 2020). However, as models develop capabilities to process more detailed information, model setup and transferability to different areas can become complicated, thus posing a challenge for more realistic, larger-scale applications (Makido et al., 2019; Ozkeresteci et al., 2003).

This study integrates Lidar-based investigation of urban forest composition with microclimate simulations in ENVI-met, bridging a critical gap in the literature by connecting object-based tree classification to the quantification of ecosystem services. While previous studies have utilized the vertical distribution of Lidar points to derive statistical metrics for tree classification (e.g., by species or structural traits) (Alonzo et al., 2014; L. Liu et al., 2017; Yu et al., 2011), most stop at the classification stage without translating these results into actionable insights about the distinct ecosystem services provided by different tree types. We follow the ideology of utilizing high-resolution, airborne Lidar point cloud data and multiple machine learning algorithms to derive metrics and classify individual urban trees based on their families and sizes. The classification results serve as a comprehensive inventory of urban forest composition, contributing to local knowledge and reducing the need for field surveys. Moving beyond, this inventory then serves as the source information for setting up the spatially explicit, object-based ENVI-met microclimate simulation models for realistic community microclimate scenarios. Despite advancements in the ENVI-met model for more explicit and detailed tree representation, no studies to date have specifically integrated tree inventories derived from remote sensing analyses to support the construction of ENVI-met simulations. Alternative urban forest scenarios are designed to quantify the composite tree cooling benefits regarding air temperature, compare the effectiveness of different trees, and predict future conditions with the presumed growth and addition of various urban trees to the community. Through this integration, we propose the workflow (Figure 1) which has the advantage of acquiring large-scale urban forest information, potentially for an entire city, and flexibly selecting areas of interest for detailed microcli-

mate simulations with automatic data input of species-specific tree models for easy setup of the target environment. The tree classification data can also serve as an inventory and the starting point for other precise quantitative measurements of urban forests' ecosystem services.

We implement this integrated workflow through a case study based on two socioeconomically different communities in Portland, Oregon, USA. We hypothesize that the taxonomical and structural characteristics of urban forests varied across different forests in various parts of the city, which would influence the effectiveness of the forests in regulating the urban microclimate. Pixel-based vegetation indices alone cannot explain this variation. Extracting, understanding, and simulating the effects of these distinct forests can help reveal the relationships between urban forests and the communities they serve, explain cross-community ecosystem service gaps. These insights provide valuable guidance for practical urban forest planning and climate adaptation strategies, emphasizing scalable solutions to address environmental inequities and enhance urban resilience. This study underscores the importance of tailored urban forest management approaches to ensure equitable access to ecosystem services across diverse communities, meeting both current needs and future climate challenges. An overview of the workflow is shown in Figure 1.

The objectives of this research are as follows:

1. To demonstrate a feasible workflow using high-resolution remote sensing data to explicit micro-scale urban environment simulation and prediction for practical urban forest planning and management.
2. To integrate object-based Lidar tree classification with ENVI-met microclimate simulation and evaluate the effectiveness of urban forests' microclimate-regulating services.
3. To identify and compare the differences in urban forest structures and compositions across different communities and observe the resulting differences in urban thermal comfort levels.

2. Methods

2.1. Study area

This study is conducted in two census tracts in the city of Portland, Oregon, USA. Portland is the second-largest city in the American Pacific

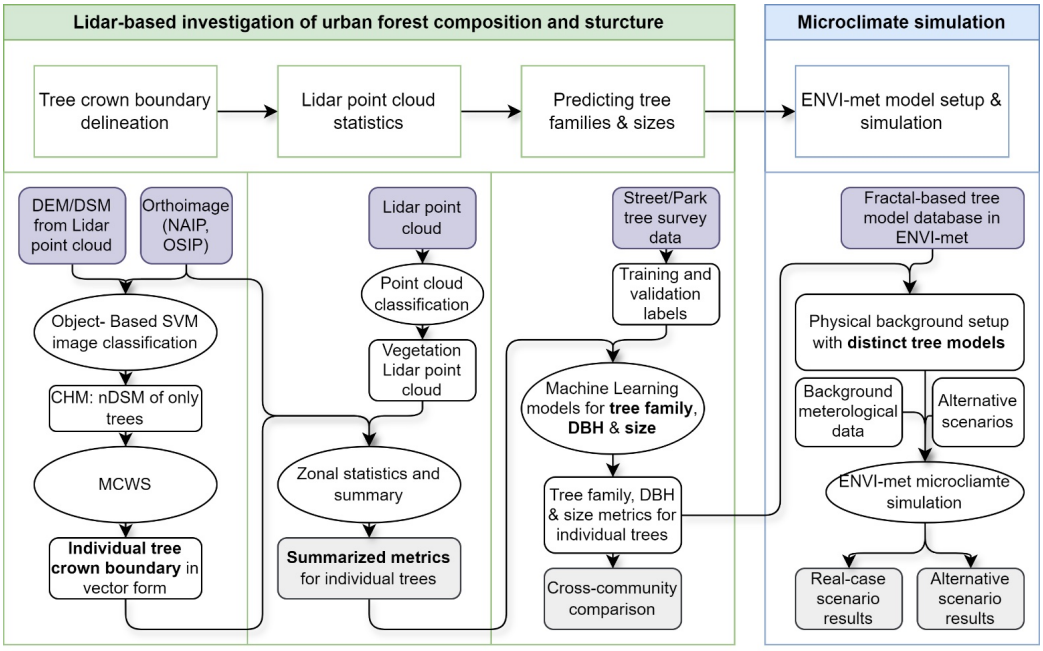


Figure 1: Research workflow. DEM: Digital Elevation Model; DSM: Digital Surface Model; NAIP: National Agriculture Imagery Program; OSIP: Oregon Statewide Imagery Program; SVM: Support Vector Machine; nDSM: Normalized Digital Surface Model; MCWS: Marker-Controlled Watershed Segmentation; DBH: Diameter at Breast Height.

Northwest, with a population of 652,503 in 2020, according to the US Census Bureau. The city is located in a warm-summer Mediterranean climate zone (Köppen climate classification: Csb) (Beck et al., 2018), with annual precipitation around 915 mm (36 inches) and mean August temperature between 16°C (60 °F) and 29°C (84 °F) (NOAA, 2021). The natural vegetation biomes in Portland include a mixture of coniferous and deciduous broadleaf trees (Franklin & Dyrness, 1973).

The two census tracts selected for this study are Multnomah County Census Tract 24.01 (referred to as Site A) and Census Tract 97.01 (referred to as Site B), which have their boundaries approved by the US Census Bureau for the 2020 census. These tracts are chosen for their representativeness of the typical American single-family house-dominated urban form and their distinct differences in socioeconomic status and urban vegetation composition. Both tracts consist mainly of single-family houses within grids of paved roads on flat topography. According to the global classification data of Local Climate Zone (LCZ), both sites are completely classified into "LCZ-6 Open low rise" (Demuzere et al., 2022). They are surrounded by similar communities in terms of urban form and LCZ classification and are at least 3.2 km (2 miles) away from major landscape features such as large natural preserves, rivers, water bodies, or densely developed downtown areas.

Site A, located in the affluent Irvington community, covers 88 hectares (211 acres). Irvington, developed between the 1890s and 1930s as a streetcar suburb, is one of Portland's early residential communities. Historically, it has been a middle- to upper-class neighborhood, offering convenient access to downtown Portland and characterized by planned urban development with intentional green spaces. Site B, in the less affluent Centennial community, covers 182 hectares (448 acres). Urbanization of this area began in the 1950s, driven by major freeway expansions and car-oriented suburban sprawl, which primarily attracted middle- to lower-class residents who could not afford higher housing prices closer to the city center. The area was annexed into the city of Portland in the 1990s. Interstate Highway I-205, a notable north-south thoroughfare, separates the city and the two sites, West (where Site A is located) and East (where Site B is located), with distinct socioeconomic characteristics. West of I-205 (with Site A as an example), communities generally have longer histories, more affluent, closer to the city center, and less vulnerable, according to the CDC's Social Vulnerability Index (SVI) (Flanagan et al., 2011). East of I-205 (with Site B as an example), communities are less affluent, further from the city center and public services,

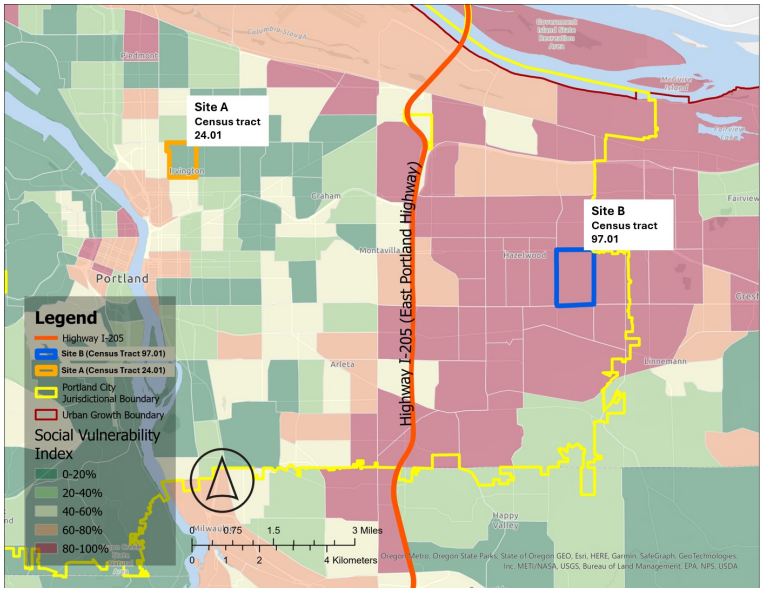


Figure 2: Locations of study sites, with Interstate Highway I-205 marked, and detail from a state-wide, highlighting the socioeconomic disparities between the two sites and the communities they represent. The background choropleth map shows the percentile of SVI scores within Oregon, with red (80%-100%) indicating the most vulnerable communities (more vulnerable than at least 80% of all census tracts in the state of Oregon), and green indicating the least vulnerable communities.

more car-dependent and more vulnerable (Figure 2).

With these distinct historical and developmental backgrounds, the two sites exhibit significant differences in their urban forest characteristics. According to American Forests, all three census block groups in Site A boast canopy coverage ratios exceeding 43%. In contrast, the four census block groups in Site B have canopy coverage ratios below 25%, making it one of the least tree-covered communities in Portland and markedly lagging behind Site A.

2.2. Individual tree crown delineation

Our first step delineates individual tree crowns. Polygon shapefiles are generated for each tree object by firstly processing the Normalized Difference Surface Models (nDSM) to create an accurate, high-resolution Canopy Height Model (CHM) that includes only valid trees, and then applying the Marker-Controlled Inverse Watershed Segmentation (MCWS) method to precisely delineate the boundaries of individual tree objects.

To achieve a tree-only CHM in the urban area, we excluded non-relevant buildings and landscape features using ArcGIS Pro's supervised object-based Supported Vector Machine (SVM) image classification tools. The primary GIS source layer is the 0.3-meter (1-ft) resolution nDSM derived from Lidar point cloud data acquired through the 2019 Portland Metro Lidar Project (Hazell, 2020). The Lidar data was collected between May 8th and August 31st, 2019. As Lidar acquisition is costly, it is not conducted annually in Portland. The 2019 dataset represents the most recent Lidar data available at the time this research is conducted. Although the City of Portland provides a lower-resolution (1-meter/3-feet) tree canopy data from simple NDVI-nDSM thresholding (Metro Data Resource Center, 2022), we need the higher spatial resolution data based on this to effectively separate non-relevant landscape features. Other input layers include airborne orthoimages and building footprints.

We first eliminate areas with pixel elevations lower than 1 meter, assuming these regions are not part of the canopy. A series of convolution kernels are applied to the nDSM and high-resolution orthoimages to prepare the input layers for segmentation and classification using machine learning models. Different layers are chosen based on their varied effectiveness in either segmentation (separating different features) or classification (identifying vegetation segments separated from other features). As shown in Table 1, we use three layers for segmentation and six layers for classification.

Table 1: : Layers for segmentation and classification steps for tree-only CHM generation

Layer name	Process	Data source
Segmentation Layers:		
Smoothed nDSM	nDSM filtered using a 3×3 convolution kernel to calculate the mean height	2019 Metro Lidar Project
Building Footprint		PortlandMaps - Open Data; Portland Bureau of Planning and Sustainability

Layer name	Process	Data source
1m Resolution Canopy Height Model (CHM) (Imperfect)		2019 Metro Lidar Project; Oregon Metro Regional Land Information System (RLIS)
Classification Layers:		
60th Percentile Height (nDSM)	nDSM filtered using a 3×3 convolution kernel to calculate the 60th percentile height	2019 Metro Lidar Project
Average NDVI from 2016 NAIP, 2018 OSIP, 2020 NAIP Images	Mean NDVI calculated from the three images	National Agriculture Imagery Program (NAIP) Oregon Statewide Imagery Program (OSIP)
Standard Deviation (nDSM)	nDSM filtered using a 3×3 convolution kernel to calculate the standard deviation	2019 Metro Lidar Project
Northward Gradient (nDSM)	nDSM filtered using a 3×3 convolution kernel to calculate the northward gradient	2019 Metro Lidar Project
Westward Gradient (nDSM)	nDSM filtered using a 3×3 convolution kernel to calculate the westward gradient	2019 Metro Lidar Project
Laplacian (nDSM)	nDSM filtered using a 3×3 convolution kernel to calculate the Laplacian	2019 Metro Lidar Project

After segmentation (Figure 3-A), during the classification phase, training samples are manually designated as either "canopy" or "non-canopy." Among the six layers prepared for classification, only one is derived from orthoim-

ages, and all others are from nDSM with convolution filters. For instance, the standard deviation filter distinguishes between vegetation and artificial structures at similar heights based on surface morphological differences. The classification results identify pixels on trees (Figure 3-B). Ultimately, we clip the original nDSM to retain only the areas representing tree canopies at a 0.3-meter (1-ft) resolution, resulting in a high-resolution CHM that contains only the canopies.

The last step is delineating individual tree crowns using the "Various Window Filter" (VWF) (Popescu & Wynne, 2004) and "Marker-Controlled Watershed Segmentation" (MCWS) (Beucher & Meyer, 1993; Münzinger et al., 2022; C. Zhang et al., 2015) with the open-source R package "ForestTools" (Plowright & Roussel, 2021). The VWF identifies treetop points representing individual trees by adjusting the search radius (window size) based on the height information of the pixels to accommodate the heterogeneous urban environment and various tree sizes. This reduces errors of both over-segmentation (where one real tree crown is delineated into several objects) and under-segmentation (where one polygon covers multiple independent real trees). MCWS then delineates tree crown polygons using the inverse watershed method. Several sets of hyperparameters (slope and intercept) are tested and adjusted until the results are deemed satisfactory upon visual comparison, and the individual tree crown object polygons are generated, as shown in Figure 3-C. When tree crown objects are generated, some preliminary parameters and geometries of the polygons are also calculated as parts of the tree's metrics for later analysis.

2.3. Lidar point cloud statistics

The airborne Lidar point cloud data are acquired with a high point density of 58 pulses per square meter on average for the study area, often resulting in more than 10,000 points for some individual trees. We use LASTools (Isenburg, 2012) for Lidar processing and zonal statistical summaries. We use the module "lascanopy", which generates zonal statistical metrics based on defined polygon boundary inputs, which are the polygons for individual trees in our study.

Before generating the metrics, we classify all points from the point cloud dataset into three classes: ground, vegetation, and building (Figure 4-D). Ground points are removed, and the remaining points are then normalized relative to the ground level to eliminate the effects of topography. Vegetation and building points are separated by leveraging the "local building planarity"

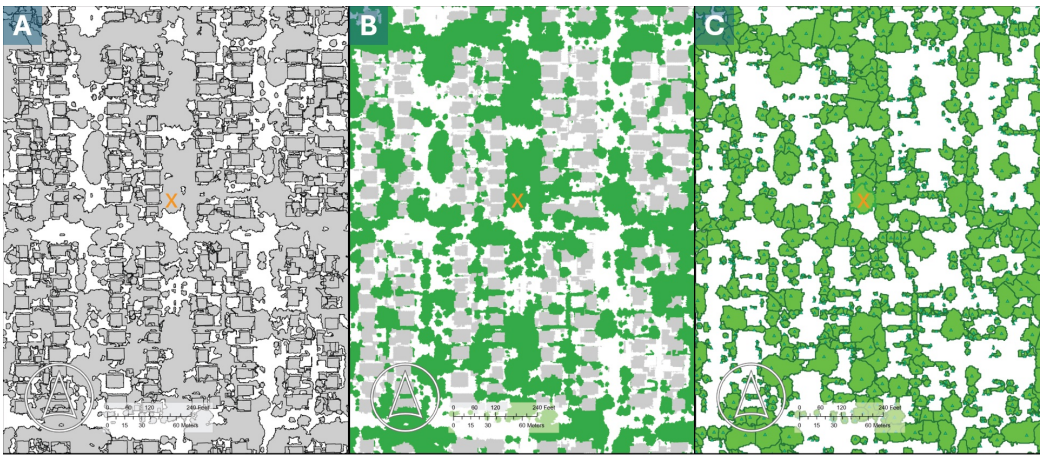


Figure 3: Sample view of tree crown delineation steps and products. The location of the sample tree (very old Norway Maple) is marked with an X. A: Segmentation, where different features are separated from one another; B: Classification, identifying areas covered by trees; C: Tree crown delineation, representing individual trees with polygon shapefiles.

and "forest ruggedness" properties of the point cloud, with default thresholding parameters set at 0.1 and 0.4, respectively. Then, all building points are further normalized to ground level to be the same as ground points, eliminating the effects on point cloud statistics for the tree's vertical structure.

With precise polygons representing individual trees, we assume that all Lidar points within the boundary of a delineated polygon are associated with the segmented tree of interest. We then built individual tree level information to provide a more comprehensive understanding of local urban forest conditions by studying the distribution of Lidar points for each tree. This step aims to generate metrics, primarily through zonal statistics of Lidar point clouds, to describe individual tree objects and support their classification and differentiation.

To separate different tree classes based on structural characteristics, we generate 52 statistical metrics of the tree canopy from the dense Lidar point cloud. See Figure 4 for a sample tree of Norway Maple from Site A. The metrics represented tree properties such as the vertical distribution of points at different height levels (Figure 4-C), point density and intensity (Figure 4-E), and relationships among different Lidar pulse returns (Figure 4-F). The varying intensities of points at different locations within a tree can reveal how laser pulses penetrate the upper canopy and reach the lower parts, providing insights into the leaf and branch structure unique to each tree (Michałowska & Rapiński, 2021). In addition, the bincentile parameters measure the fraction of points beneath a certain percentile of the tree's total height (e.g., 50% bincentile means the fraction of points reflected below 50% of the tree's height). Higher bincentile values across the metrics profile indicate more points are returned in the lower sections of the tree, suggesting a cone-shaped, coniferous tree. Conversely, lower bincentile values indicate more points are trapped in the upper parts of the tree crown, suggesting most biomass is concentrated in the dense upper parts where most Lidar pulses are returned, with few penetrating lower (Yu et al., 2011). For the 52 metrics, 43 are summarized from Lidar point cloud statistics, with 9 supplementary metrics derived from interpreting different bands from orthoimages. This combined information can be utilized to reveal and distinguish different trees. See Appendix-1 for the full list of metrics for individual tree descriptions.

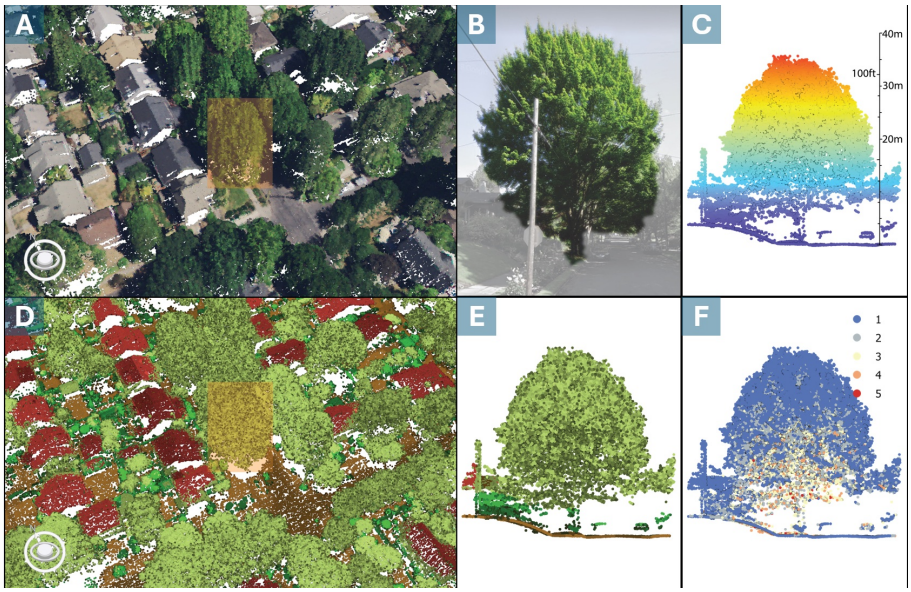


Figure 4: (A) Relative location of the sample tree in the neighborhood, displayed as Lidar point cloud colored by NAIP imagery. (B) Sample tree in Google Street View. (C) Sample tree Lidar point cloud with color indicating relative elevation from the ground. (D) Relative location of the sample tree within the classified Lidar dataset. (E) Sample tree Lidar point cloud with color representing point intensity. (F) Sample tree Lidar point cloud with color denoting point returns.

2.4. Predicting tree families and sizes with machine learning

This step utilizes machine learning models to predict the family, diameter at breast height (DBH), and sizes of every tree object within the study scope, including those on private lands, regardless of accessibility for ground truth measurement. Machine learning classifiers are trained on the metrics for individual trees, with training and validation labels from the City of Portland's street tree and park tree survey data (DiSalvo et al., 2017; Portland Parks & Recreation, 2021). The survey, conducted between 2011 and 2019 as part of the city's tree inventory project, collected data through ground measurements carried out by professional arborists and supported by volunteers. The survey data is supported by citizen science and many volunteers on trees within the public domain, including roadside trees and trees in urban parks. Each surveyed tree includes parameters such as species, family, coniferous/deciduous status, DBH, and height, providing data for more than 200,000 trees within the city, which is a comprehensive database, but still incomplete and impossible for recording every tree within the city.

Two surveyed parameters are selected as the targets for machine learning model prediction: tree family (categorical) and DBH (numerical). The predicted DBH is then input into unsupervised clustering studies with other parameters from the metrics for tree size clustering. Different tree families may show significantly different structural, morphological, and biological features, which can be reflected in the metrics. This study assumes that species within the same family share similar appearance and biophysical characteristics, allowing them to perform comparable ecosystem functions in adjusting the microclimate for subsequent analyses (S. Kim et al., 2011). This allows us to have a reasonable amount of classes, as too many classes would impact the overall accuracy and would increase the risk of having an imbalanced sample size in accuracy computation due to different abundances of various species (Voss & Sugumaran, 2008). We determine seven representative and dominant classes of vegetation, including six families of trees based on analyzing the tree survey data for dominant families within the study scope, and one class for all other shrubs and hedges. Each of the six selected tree families has at least 60 valid training samples from the survey data from the two study sites combined. While shrubs and hedges are not included in the survey dataset, we use them as labels in a set of training samples that is manually selected by interpreting orthoimages and nDSM. The structural and taxonomic properties of shrubs are of less interest to this study and are thus only simply summarized and later treated as pixel-based vegetation in

microclimate simulations (i.e., Section 2.5). Rarer families with fewer than 40 surveyed samples are not included due to insufficient training data, and those trees belonging to these rarer families are classified into other more dominant families. While this introduces selection bias, it is deemed reasonable to simplify the prediction and microclimate simulation, and the selected families can represent various dominant tree types within the study scopes. Each georeferenced tree survey record is spatially joined with a tree crown polygon object at that location. We then manually filtered the training dataset by the quality of delineation and preciseness of the survey location's coordinates and eliminated the mismatches. In total, 1,303 survey records are used for training and validation purposes, including 274 manually created shrub labels. 1,029 of them are from tree survey data, which accounts for 30.4% of the survey records that exist within the study scope (3,385 in total) (Table 2).

The second variable is diameter at breast height (DBH, which is associated with trees' size and age). Although it is challenging to measure DBH through remote sensing, DBH is believed to be strongly correlated with other parameters that can be summarized with Lidar point cloud statistics, such as crown area, tree height, and vertical profile metrics. This makes DBH suitable for machine learning experiments, following similar procedures to those used in tree family classification, but this time as a numerical prediction study, excluding shrub/hedge.

Table 2: Select tree families and the shrub class for individual tree object classification.

Families	Representative species	Number of training samples	Notable characteristics	Representative tree model species in ENVI-met
Sapindaceae	Maple	467	Large broadleaf deciduous	"Norway Maple"
Rosaceae	Cherry, Apple, Plum, Peach	260	Medium broadleaf deciduous	"Wild Cherry 'Plena' "

Families	Representative species	Number of training samples	Notable characteristics	Representative tree model species in ENVI-met
Betulaceae	Alder, Birch	85	Large broadleaf deciduous	"Hanging Birch"
Pinaceae	Pine, Fir, Spruce	78	Large coniferous evergreen	"Pine Tree"
Fagaceae	Chestnut, Oak	75	Large broadleaf deciduous	" 'Pedunculate' Oak"
Cornaceae	Dogwood, Dove tree	64	Medium broadleaf deciduous	"Swedish Whitebeam"
Shrub/Hedge	All shrub	274	Limited potential to grow large	Rasterized shrub pixels
Total		1303		

For tree family classification and DBH prediction, we compared machine learning models from Scikit-learn (Pedregosa et al., 2011) including Random Forest (RF), Linear Regression, K-means, and Support Vector Machines (SVM). For each test, 80% of the training samples are used for training and 20% for validation, respectively. To avoid class imbalance, underrepresented families are oversampled (Chawla et al., 2002). The experiments are bootstrapped 1,000 times to compare either the average classification accuracy for family classification or Root Mean Square Error (RMSE) for DBH regression with 95% confidence interval (Efron, 1979). For family classification, five rounds of cross-validation are conducted for each classifier, each time using a different 20% of the samples for validation and 80% for training, and with combined accuracy metrics generated for results presentation (Stone, 1974).

The final step involved canopy size clustering. For larger tree canopies other than shrubs and hedges, the goal is to classify them based on their family and size for later microclimate simulation. Tree sizes are determined using unsupervised clustering on three parameters: DBH, height, and crown area. After normalizing these parameters, the height parameter is weighted by a factor of 2. The K-means clustering method is used to group the trees into four clusters, whose names are "young trees," "middle-aged trees," "old trees," and "very old trees," given the strong correlation between age and size. This clustering scheme corresponds to the tree size categories used during the

microclimate simulation in Section 2.5, so trees of different sizes have different models to represent them. Classified shrubs are separated from other trees and classified as "tall" (higher than 3 meters) or "short" (lower than 3 meters) based on nDSM thresholding. By the end of this step, each tree is classified by family and size, creating an inventory of urban tree composition. This inventory facilitates cross-community density comparisons of different trees and supports the microclimate simulations introduced in Section 2.5.

2.5. Microclimate simulation with ENVI-met

The microclimate simulation is conducted using the ENVI-met model with only one computer core, limiting the ability for large-area simulations. To demonstrate feasibility, the simulation area is reduced to four urban blocks bounded by streets in the middle of each study site (5.7 hectares, or 14.0 acres in Site A, 6.9 hectares, or 17.2 acres in Site B). However, the automatic classification of all trees in our study area enables the method to be applied to larger areas. Using the Space and Albero modules of ENVI-met, we integrate our urban tree classification results and automatically constructed a 3D model for each site, rather than assigning individual trees manually. The Albero module manages distinct individual tree models. The module allows users to create detailed, tailored tree models utilizing fractal-based L-String logic and algorithms that represent various types of vegetation with user-defined structural and biophysical parameters (Simon et al., 2020) (See Figure 5-B for an example). It also includes a predefined database of many existing tree models representing different species and sizes, from which many of the tree models in this study are derived.

For different tree families, a representative species model is selected from the Albero database (Table 2). An exception is made for the Cornaceae family, for which the Swedish whitebeam tree model is substituted. This substitution is made because the Swedish whitebeam shares similarities with Cornaceae trees, such as dogwood trees, especially in terms of size. Since Cornaceae trees are relatively rare compared to other families within the study scope, this substitution is deemed reasonable and unlikely to affect the results significantly. For each tree, the Albero module provides models of the same species in different sizes: "young," "middle-aged," "old," and "very old," corresponding to the tree size clustering results. The experimental setup for shrubs and hedges involved representing them as either "4-meter-high hedge" for the "tall shrub" class or "2-meter-high hedge" for the "short shrub" class.

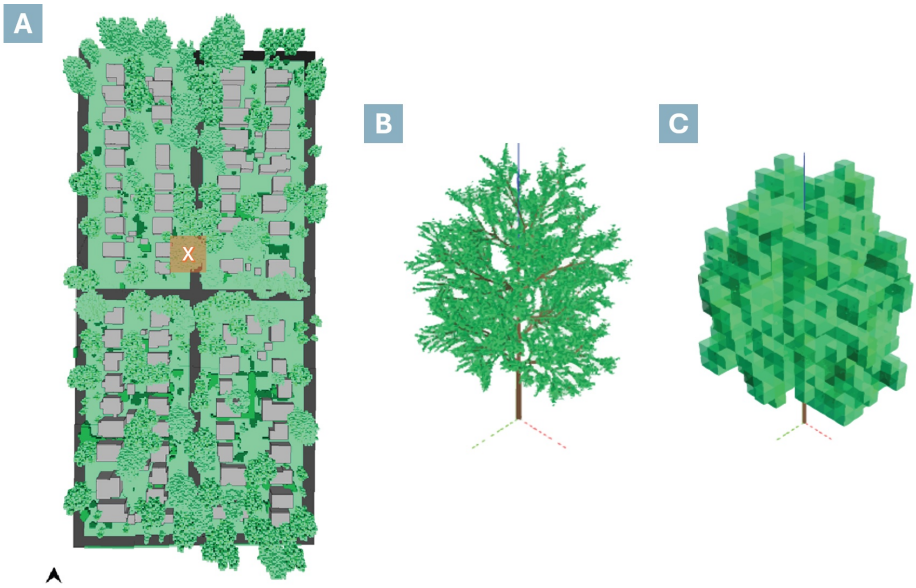


Figure 5: (A) Ortho-view of the ENVI-met model setup for the selected simulation area of site A, with the location of the sample old Norway Maple tree marked as "X". (B) The L-String model of "X" from Albero database. (C) The voxelated model of "X" during simulations.

To focus on comparing the mitigation effects of different trees on the microclimate, this study simplifies other aspects of the model's setup. Building footprints are established using OpenStreetMap data, and all buildings are modeled as single-family homes with default concrete materials. Soil can significantly impact the microclimate due to differences in thermal conductivity and water-holding capacity. "Silty loam soil" (ID: 0000SO) under hydrologic group B is chosen for both sites, with a layer of simple lawn added on top, referencing Soil Texture data from the Conservation Biology Institute. "Asphalt road" (ID: 0100SL) is assigned to be the paving material for every street. See Figure 5 for a sample view of the model setup at 1-meter resolution for Site A (the highest resolution available for the model), with the location of the sample old Norway Maple tree marked as X, and its detailed setups. The simulation is set to run from August 5th at 5 AM (sunrise) to August 6th at 5 AM, covering a full 24-hour period, which is a typical hot summer day in Portland with relatively high temperature and mild wind speed.

To reduce computational demand after setting up the 1-meter resolution

model, the horizontal and vertical resolutions are resampled to 3 meters, respectively, for spaces below 12 meters in elevation. The space between 0 and 3 meters is further divided into 0.6-meter grids vertically for more granular near-ground simulation. Vertical spaces over 12 meters are divided using coarser telescoping grids (each grid 30% higher than the one below it) until 30 meters. The ENVI-met model also automatically adds 5-cell (15-meter) horizonal buffer zone surrounding the site on each lateral boundary to minimize boundary effects. During this process, the tree models are voxelated from their detailed fractal-based digitization, with an example shown in Figure 5-C.

Six series of simulations are designed, as shown in Table 3. These simulations aim to evaluate the microclimate regulation benefits of urban trees and demonstrate the model's applicability in both real-world and hypothetical planning scenarios. Each serves one of the three purposes, which are real case scenario, model sensitivity tests, and alternative planning.

Scenario #1 uses realistic tree models derived from machine learning classification to simulate the current conditions of Sites A and B. This baseline scenario provides a foundation for comparing the effects of other scenarios.

Scenario #2, referred to as the "No Tree" scenario, serves as a sensitivity test by removing all trees from the simulation model while retaining other landscape features. The temperature differences between Scenario #2 and Scenario #1 quantify the combined microclimate-regulating effects of the entire urban forest. Scenario #3 focuses on Site A and involves the removal of a single mature Norway Maple from the center of the simulation area. This sensitivity test evaluates the localized impact of an individual tree on the microclimate and demonstrates the stability of the ENVI-met model. By isolating the effect of removing one tree, this scenario ensures that areas distant from the removed tree remain unaffected, validating the model's reliability. Scenarios #4-1 and #4-2 further explore the role of tree species by replacing all trees in Sites A and B with either Maples (broadleaf deciduous) or Pines (evergreen coniferous) without altering tree sizes. While these scenarios are not grounded in real-world conditions, they enable comparisons of the microclimate regulation benefits of different species based on ENVI-met's species-specific models.

Scenario #5 models a plausible future growth trajectory for the urban forests in both sites. This scenario assumes that most "young" and "middle" size trees will grow into "old" sizes, and "old" trees will grow into "very old" sizes, except for Rosaceae and Cornaceae, which are biologically constrained

to reach only "middle" sizes. This projection examines how natural growth of existing urban forests could influence long-term microclimate regulation, offering a realistic vision of the future without significant new tree additions. Scenarios #6-1 through #6-4 simulate the addition of 40 trees of different conditions to Site B, reflecting Portland's ongoing efforts to increase urban forest coverage. These scenarios are inspired by local street tree inventory reports, which identify potential planting sites and advocate for long-term effective planting practices. Scenarios #6-1 and #6-2 compare the impacts of planting 40 "young" Maples versus 40 "young" Cherries in similar open front yard locations. Scenarios #6-3 and #6-4 assess the benefits of these newly planted trees as they grow, with Maples maturing into "old" sizes and Cherries limited to "middle" sizes. These alternative planning scenarios emphasize the importance of selecting effective tree species and the critical role of sustained maintenance in ensuring trees grow to their full potential, thereby maximizing microclimate benefits.

Simulation results were visualized and analyzed using the ENVI-met Leandro module.

Table 3: List of scenarios designed and independently simulated with ENVI-met for both study sites

Scenario #	**Simulation Name**	**Simulated Sites**	**Purpose**	**Explanation**
1	Real case	A, B	Real case scenario	Realistic tree models derived from machine learning classification.
2	No tree	A, B	Sensitivity test	All landscape features remained but no trees, to quantify the combined microclimate-regulating service of all trees.
3	Remove one tree	A	Sensitivity test	Removal of an old Norway Maple to isolate the impact of a single tree.
4-1	All maple	A, B	Sensitivity test	Replace all trees with Maples, without altering sizes, to test species differences in ENVI-met tree models.

Scenario #	Simulation Name	Simulated Sites	Purpose	Explanation
4-2	All pine	A, B	Sensitivity test	Replace all trees with Pines, without altering sizes.
5	Future: after growth	A, B	Alternative planning	Predict future forest structure, assume all trees of "young" and "middle" sizes can grow to old size and trees of "old" size can grow to "very old" size, exceptions are Rosaceae and Cornaceae that can only grow the "middle" size.
6-1	Add 40 young maple	B	Alternative planning	Plant 40 young Maples in front yards of houses with open spaces.
6-2	Add 40 young cherry	B	Alternative planning	Plant 40 young Cherries in similar locations.
6-3	Add 40 old maple	B	Alternative planning	Assess the impact of 40 Maples growing into old trees, as Maples have the potential to grow very large
6-4	Add 40 middle cherry	B	Alternative planning	Assess the impact of 40 Cherries growing into middle-size trees, as Cherries do not have the potential to grow large

3. Results

1.

3.1. Tree family classification

We generated the individual tree polygons as shown in the example in Figure 3-C. There are 12,912 identified tree objects from both sites combined: 5,470 are from Site A, and 7,442 are from Site B. This corresponds to densities of 62.0 and 40.8 trees per hectare at Site A and B, respectively.

After testing multiple machine learning models, Random Forest (RF) is determined to be the most accurate for both tree family categorical classification and DBH numerical prediction. For tree family classification, with hyperparameters set to 100 estimators and using the "gini" criterion, the RF model achieved an average classification accuracy of 67.1%. After bootstrapping, the 95% confidence interval is determined to be between 61.6% and 72.6%, significantly higher than the random guessing null hypothesis accuracy of 22.8%. Among the 52 metrics, "Min_Slope" (minimum slope of the upper tree crown surface), "Z_Mean_FirstReturn" (mean height of the first return), "LastofManyre" (count of last of many returns), and "averageNDVI" had the highest importance scores, which are all above 0.03, suggesting they are relatively important among all metrics in splitting the data during the RF classification (Appendix-1).

After cross-validation analysis, the combined classification confusion matrix is shown in Figure 6 and the classification scores are in Table 4. The classification accuracies achieved an overall Cohen's Kappa (k) value of 0.59, indicating moderate agreement. The accuracy varied among families, with the Shrub class achieving the highest F1-score of 0.85, followed by Sapindaceae (0.77), Pinaceae (0.62), and Rosaceae (0.60). Shrub has the highest accuracy, likely due to its fundamental structural differences from other canopy classes. Sapindaceae may be overfitted during the training process due to the higher number of samples, although oversampling is performed on underrepresented families. Pinaceae's accuracy is also higher since it is the only coniferous evergreen tree family in this study, in contrast to the other broadleaf deciduous tree families, which may share some similarities.

In contrast, Fagaceae (0.49), Betulaceae (0.43), and Cornaceae (0.38) have relatively low F1-scores. These lower F1-scores are primarily due to class imbalance and low recall values. Shrub, Sapindaceae, and Rosaceae exhibited relatively balanced metrics, with higher recall than precision. On the other hand, Pinaceae, Fagaceae, Cornaceae, and Betulaceae showed lower recall values compared to precision. Specifically, Fagaceae (0.38), Cornaceae (0.28), and Betulaceae (0.29) had recall values lower than 0.40. For example, Betulaceae had a Precision of 0.81 but a much lower recall of 0.29, suggesting that the model could avoid false positives but suffered from many false negative cases. This indicates that many actual Betulaceae trees are misclassified into other families, particularly Sapindaceae and Rosaceae. In contrast, few trees from other families are inaccurately classified as Betulaceae trees, likely due to the lack of valid samples.

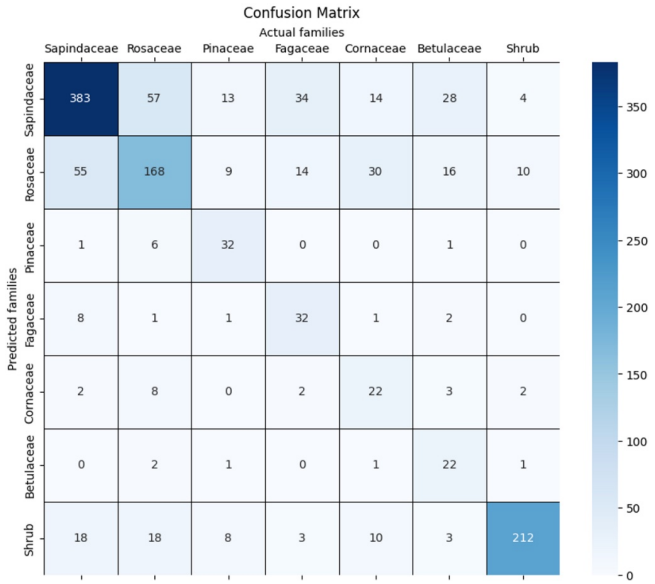


Figure 6: Confusion matrix for tree family classification with Random Forest classifier trained with cross-validation.

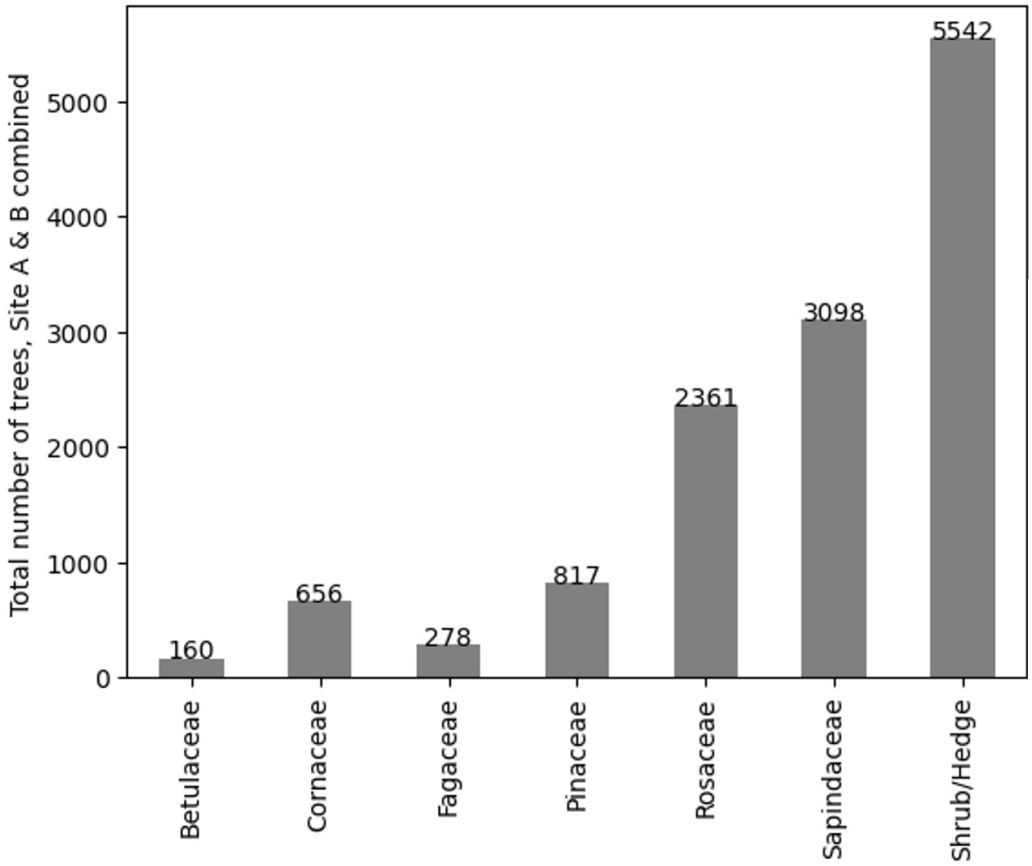
Table 4: Precision, Recall, F1-Score and Support for the Random Forest classifier trained with cross-validation

Class	Precision	Recall	F1-Score	Number of samples
Sapindaceae	0.72	0.82	0.77	467
Rosaceae	0.56	0.65	0.60	260
Pinaceae	0.80	0.50	0.62	64
Fagaceae	0.71	0.38	0.49	85
Cornaceae	0.56	0.28	0.38	78
Betulaceae	0.81	0.29	0.43	75
Shrub	0.78	0.93	0.85	229

We then used this trained RF model to predict the tree family properties of all 12,912 tree objects within the two study sites, and the total numbers of trees from each family from both sites are summarized in Figure 7-A. There are 5,633 shrub objects, more than any other family of large trees. The most abundant actual tree families are Sapindaceae and Rosaceae, with 3,010

and 2,390 counts, respectively. These two families also have more training samples than the others (467 for Sapindaceae and 260 for Rosaceae). For the remaining families, there are more Pinaceae and Cornaceae trees (800 and 630) than Fagaceae and Betulaceae trees (289 and 160), even though they have similar amounts of training samples.

With the classification results, we compared the distribution of different families of trees in our two study sites, specifically the density (number of trees per hectare) of each family of trees (excluding shrubs, as they do not refer to actual trees). Site A generally has a much higher density of trees than Site B. It has more than twice the density of Sapindaceae trees compared to Site B (18.0 per hectare at Site A compared to 7.8 per hectare at Site B), significantly higher densities of Fagaceae and Betulaceae trees, a similar density of Rosaceae trees, and a lower density of Cornaceae and Pinaceae trees (Figure 7-B).



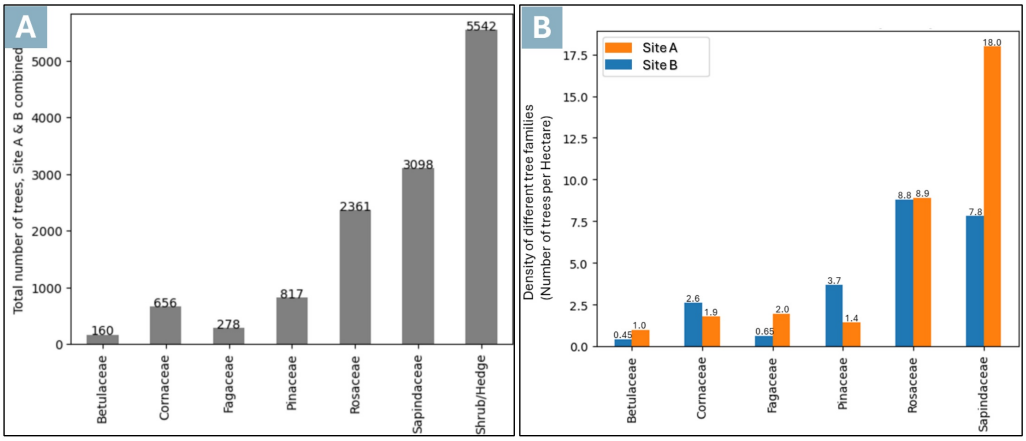


Figure 7: (A) Total number of predicted trees for each family, combined from both Site A and Site B. (B) Comparison of tree density (number of trees per hectare) for the six real tree families between Site A and Site B.

3.2. DBH prediction and tree size clustering

RF is also chosen to predict Diameter at Breast Height (DBH). For hyperparameters, we set the number of decision trees at 100 and the criterion to "squared error." Comparing the regression results to actual DBH measurements, the overall coefficient of determination (R^2) is observed to be 0.79. The mean Root Mean Square Error (RMSE) is 12.88 centimeters (5.07 inches), with a 95% confidence interval for the RMSE between 10.92 centimeters (4.34 inches) and 14.70 centimeters (5.79 inches) after 1000 bootstraps (Figure 8-A). The trained RF model is then used to predict the DBH for all trees. The overall mean DBH for all six families of trees is 36.83 centimeters (14.50 inches), and the standard deviation is 24.94 centimeters (9.82 inches) (Figure 8-B).

The predicted DBH information is further used to classify the sizes of all six tree families, excluding objects already classified as shrubs in the tree family classification stage. Using the predicted DBH, along with other parameters such as tree height and crown area, all trees are clustered using the unsupervised K-means model into four clusters: "young," "middle," "old," and "very old." The clustered objects are separated into the six tree family classes, and a 3-dimensional plot is generated for each family, as shown in Figure 9. Sapindaceae and Betulaceae exhibited visually even distributions of tree objects of all sizes. In contrast, Rosaceae and Cornaceae trees are

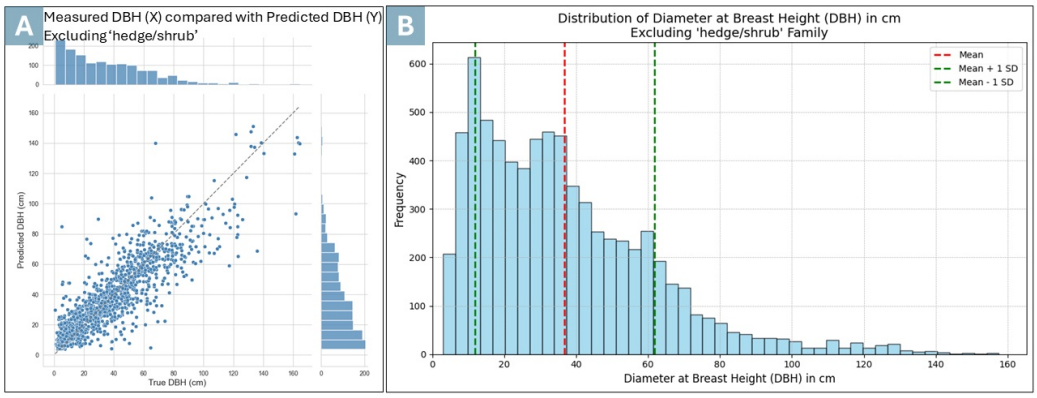


Figure 8: (A) DBH prediction results compared with actual measurements from validation samples. (B) Distribution of DBH for all trees from both study sites.

primarily within the ”young” and ”middle” classes, with no samples in the larger size groups. Pinaceae trees tended to be relatively larger, with a higher likelihood of being clustered as ”old” and ”very old.” Fagaceae trees are either ”young” or ”very old,” with a noticeable lack of samples in the ”middle” size class.

Combining the tree family classification and tree size clustering information for each tree, we generate community tree maps for both study sites to reflect these two properties for every individual tree object within the study scope (Figure 10). As the two maps are displayed at the same scale, visual comparison reveals that Site A has a much denser and larger tree population, covering more area within the community than Site B, where trees are sparser and smaller. Furthermore, the color coding indicates that Site A has a higher density of Sapindaceae and Fagaceae, both of which mainly consist of large broadleaf deciduous trees. At the same time, Site B is visually more abundant in Pinaceae trees, a coniferous evergreen family. Individual tree polygons also tend to be larger in Site A than Site B, indicating a greater presence of “old” and “very old” trees together with the color gradient.

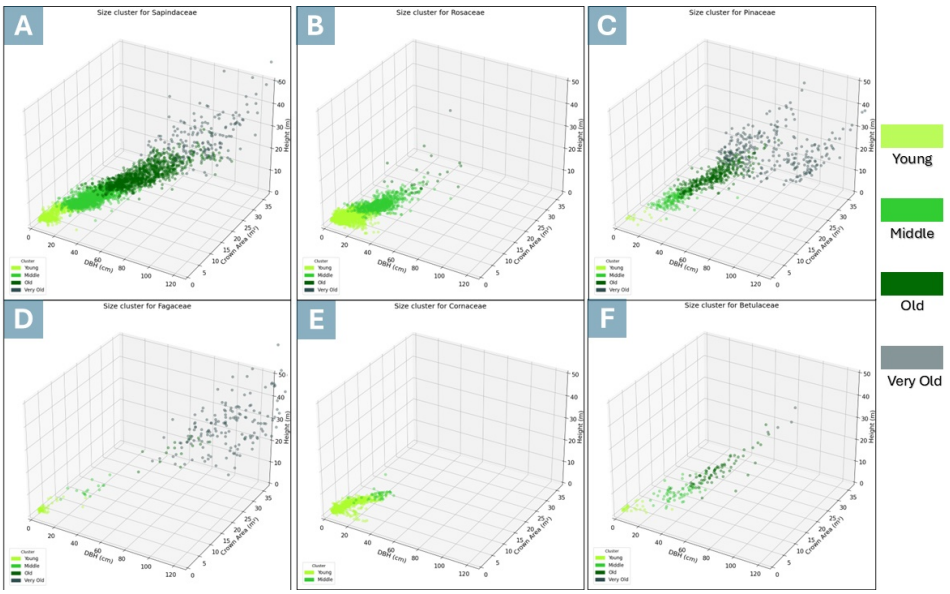


Figure 9: Tree size clustering results for each tree family: (A) Sapindaceae; (B) Rosaceae; (C) Pinaceae; (D) Fagaceae; (E) Cornaceae; (F) Betulaceae.

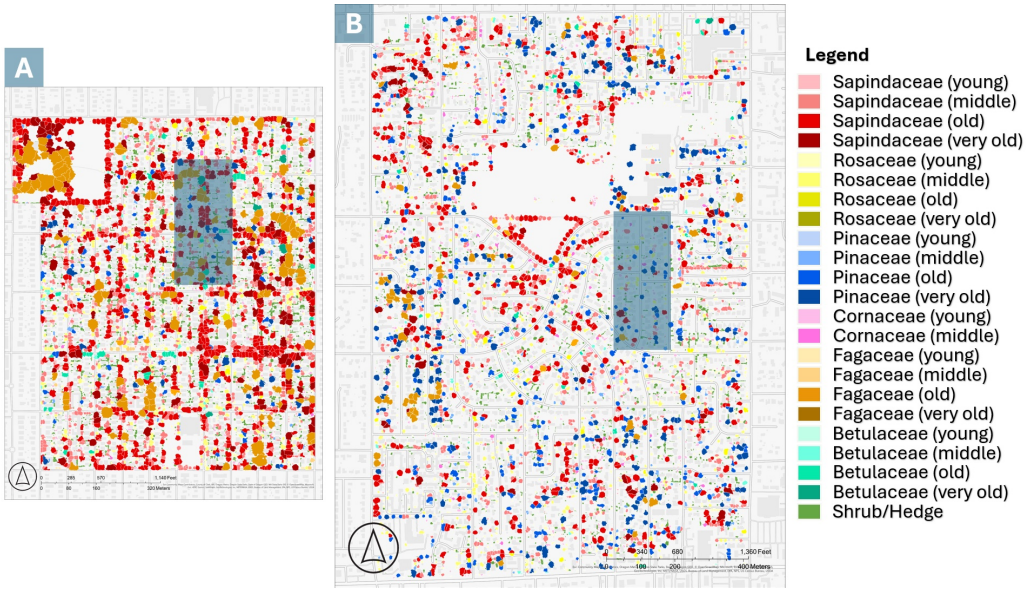


Figure 10: Tree family classification and size clustering results. Both maps are on the same scale. Colors represent different tree families, and gradients represent tree sizes. Shaded areas indicated the selected regions for microclimate simulation analyses. (A) Site A; (B) Site B.

3.3. Microclimate simulation and scenario testing

We conduct 15 independent simulations using ENVI-met to explore various scenarios, including real-case scenarios (Scenario #1), sensitivity testing scenarios (Scenario #2, 3, 4-1, and 4-2), and future projection scenarios (Scenario #5, 6-1 to 6-4). The simulations focused on a small subset of each study site (four blocks per site), as shown in Figure 10. Each simulation run takes approximately two full days to process on a single CPU core of a standard personal computer (11th Gen Intel Core i5 CPU @ 2.40 GHz, 4 Cores, 16GB RAM). The simulation outputs included a variety of microclimate variables such as atmospheric air temperature, humidity, airflow speed and direction, radiation at different elevations, soil properties (including soil moisture and land surface temperature), and object-specific properties (such as roof/wall temperature and vegetation temperature).

For this study, we chose air temperature at 1.5 meters above ground level to demonstrate site-specific findings and compare different sites and scenarios. This elevation reflects the air temperature experienced by an average adult and is considered a more suitable indicator for evaluating local climate and heat stress compared to land surface temperature (LST) (Almeida et al., 2021; Chakraborty et al., 2022). We select the conditions at 4 PM local time for each scenario, as this time best reflects the contributions of vegetation to the microclimate after a full day of intense solar radiation and heat.

The simulation results of the real-case scenario (Scenario #1), which is set up with the objective tree classification and clustering data generated from previous steps, are shown in Figure 11. Comparing Sites A and B, the air temperature between the coolest and hottest locations at 4 PM differed by 0.81°C (K) for Scenario #1. The minimum, maximum, and median temperatures for Site A (23.18°C, 23.76°C, and 23.45°C, respectively) are all lower than those for Site B (23.46°C, 23.99°C, and 23.68°C, respectively) by around 0.2 to 0.3°C (K). The temperature difference may be influenced by the varying tree compositions. For each census tract, the west and south edges are simulated to be hotter than other places, which can be due to the model's edge effects and the wind direction at and prior to 4 PM (northwest wind). Overall, the Scenario #1 simulations reflect the impact of vegetation on microclimate, as areas below or near trees or tree clusters exhibit lower air temperatures and thus experience less thermal stress. It is worth noting that the western portion of Site A appears to be hotter. This is likely due to the prevailing wind direction from the northwest in the background weather at the time of the simulation. The elevated temperatures in this area may

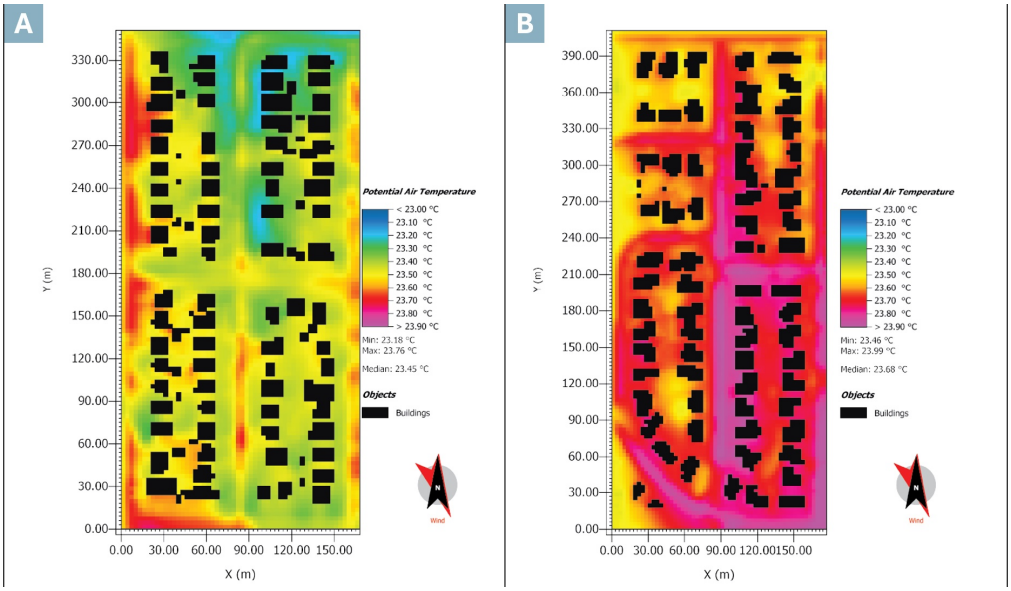


Figure 11: Real-case scenario, potential air temperature at 1.5 meters above ground at 4 PM on a typical summer day. Temperature unit: Degree Celsius (°C) (A) Site A; (B) Site B.

primarily reflect the hotter conditions of the background weather without any cooling influence from neighboring landscapes beyond the study area.

The sensitivity tests revealed more about the different effects of individual tree objects in the ENVI-met model. In Scenario #2 (Table 3), we calculate the difference between the "No tree" scenario, where all trees are removed from the model, and Scenario #1. This approach quantifies the combined microclimate regulating services of all the trees within the community and allows for comparison of these services across different communities (Figure 12). Removing the urban forest in Site A would increase the air temperature by an average of 0.22°C (K), with some locations experiencing increases up to 0.53°C (K). This indicates that Site A's forest provides more significant cooling services than Site B, where the average air temperature would increase by only 0.05°C (K). The model even allows for more precise quantification of the microclimate regulating effects of individual trees. In Scenario #3, we remove a single "old Norway maple" from the center of Site A's simulation model and compared the results to Scenario #1. The results showed an ambient temperature difference of 0.18°C (K), while other areas remained unchanged (Appendix-2.1). We further tested the cooling effectiveness of different tree

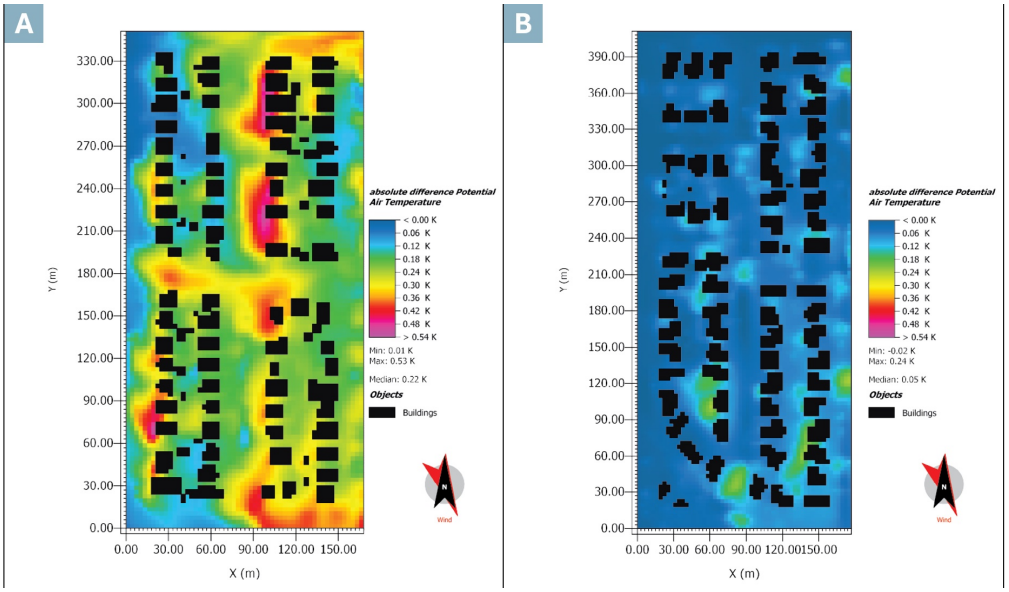


Figure 12: "No tree" scenario (Scenario #2) compared to the real-case scenario (Scenario #1), showing potential air temperature at 1.5 meters above ground at 4 PM on a typical summer day. If all trees are removed, the air temperature will rise at both sites, with a more significant increase at Site A. Temperature units: Kelvin (K) or Degree Celsius (°C). (A) Site A; (B) Site B.

models by converting all trees into either Norway maple (Sapindaceae, Scenario #4-1) or pine (Pinaceae, Scenario #4-2). The temperature differences compared to Scenario #1 indicated that Norway maple is generally more effective than pine in cooling the environment, with both sites experiencing an additional 0.10°C (K) cooling effect. Conversely, converting all trees to pines resulted in a hotter environment for both sites, particularly for Site A, where the average temperature increased by 0.19°C (K) due to the high density of Sapindaceae trees originally present. These results suggest that Sapindaceae trees are more effective and thus preferable to Pinaceae trees for microclimate regulation services (Appendix-2.2).

Lastly, we simulate different future alternative scenarios. For Scenario #5, although no new trees are added, tree sizes are amended based on their projected growth potential for different families (Refer to Table 3). The simulations suggest that, following the current growth trajectory, the existing combination of urban forests would offer increased cooling benefits. Site A would experience a greater net benefit gain than Site B, with the potential

to reduce temperatures of 0.11°C (K) on average, compared to an average cooling of 0.07°C (K) in Site B, despite Site A already enjoying more benefits than Site B (Appendix-2.3). Scenarios #6-1 to 6-4 all assume the addition of 40 trees to Site B. As newly planted trees are small, neither planting Norway maple nor cherry trees would provide immediately noticeable extra cooling benefits compared to the status quo (maximum is 0.03°C (K) for maples and 0.02°C (K) for cherries), and the temperature would not change significantly. However, as time progresses, Norway maples are projected to grow into "old" trees, significantly reducing the air temperature as high as 0.37°C (K) compared to cherry trees, which would only reduce temperatures as high as 0.16°C (K), as they are only able to grow to "middle" sizes (Appendix-2.4).

4. Discussion

This study explores a workflow integrating object-based urban tree classification with 3D microclimate simulation. Utilizing high-resolution airborne Lidar data, we classify and predict properties for individual trees in terms of family, DBH, and size. We used these results to create an urban forest inventory, which is then input into the ENVI-met model to set up community-scale 3D physical environment models with distinct tree models for microclimate simulations and alternative scenario testing. The workflow is demonstrated through a case study of two residential areas in Portland, similar in urban form but differing in socioeconomic status. This study not only illustrated a specific use of Lidar and urban forest data but also showcased the workflow's adaptability for similar studies in different areas, integrating urban tree analysis with ecosystem services modeling, with the potential to extend to more places with available Lidar and ground labeling data. In addition, the case study revealed meaningful insights into the structure and classification of urban forests at the individual tree level and their composite effects on the urban microclimate. It highlighted the differences and inequalities in urban forest service, offering a deeper understanding of cross-community equity issues and facilitating the tests of alternative scenarios for improvement.

The case study revealed that the two socioeconomically distinct communities in Portland differ in vegetation abundance and urban forest composition. The more affluent community had a denser distribution of larger broadleaf deciduous trees (Sapindaceae, Fagaceae, and Betulaceae), which are theoretically more beneficial for urban climate regulation due to more substantial evapotranspiration potential. Conversely, the less affluent com-

munity had relatively more Pinaceae and smaller broadleaf trees (Rosaceae and Cornaceae), limiting not only the current but also the future potential for microclimate regulation if current trend continues. The study results suggest that socially vulnerable communities can experience greater benefits from their urban forest, if tree planting is increased and if tree selection is improved to build a resilient, effective urban forest composition for long-term benefits. A common challenge is that lower-income communities may avoid larger tree species due to concerns about yard space, maintenance, and potential risks like falling branches despite getting trees for free. These socioeconomic and cultural preferences are critical in developing urban forest strategies (Nguyen et al., 2017; Roman et al., 2018). Further research is needed to design interventions that balance ecological and social factors.

4.1. Urban tree properties with Lidar and machine learning

This study summarized individual tree properties using Lidar-derived metrics and machine learning classifiers. The result can serve as a comprehensive inventory of all urban trees and support other physical modeling or ecosystem services quantification analyses within the study scope, not limited to microclimate simulations experimented in this study. When inventories from multiple years are available, comparisons can be conducted to investigate both quantitatively and qualitatively how the urban forests have evolved, reducing the need for time consuming ground surveying and data acquisition (Coops et al., 2021).

Given the heterogeneous urban environment of the study sites, the original nDSM can not be directly interpreted as a tree-only CHM. Significant data cleaning and image processing work is necessary before tree delineation. Despite over- and under-segmentation during tree delineation, particularly in the more complex structure of Site A, each delineated polygon is interpreted as one tree object, which is considered reasonable for heterogeneous urban areas as experienced in Münzinger et al. (2022) and C. Zhang et al. (2015). However, there are other more complex methods attempting more accurate segmentation, such as the vector-based concave hull methods applied directly to the original point cloud without conversion through nDSM, which are worth trying for future studies (Jakubowski et al., 2013).

When generating the metrics for trees, some metrics are easily interpretable and comparable across different trees, such as the spectral metrics and the percentiles (the height of specific percentiles of points from the bottom). Some others are more intricate and harder to comprehend directly

and individually. For example, "hom," or "Height of Median Energy," is one of the statistical concepts of the distribution of the points, which is hard to associate directly with the shapes of canopies. It is also hard to compare a single bincentile metric without comparing the whole series. By comparing the whole series of bincentile metrics among different trees, we observed that some trees, regardless of size, have more returns concentrated on the upper parts of the tree crown than others. This can be due to denser leaves in the upper crowns, suggesting these trees are likely broadleaf deciduous with spherical crown shapes and dense foliage rather than cone-shaped coniferous trees, thus aiding the differentiation of tree classes. Further literature consultation reveals that Lidar point clouds can also be used to derive other critical biophysical properties, such as Leaf Area Index (LAI) (Tian et al., 2021; Zhu et al., 2018), a key factor influencing evapotranspiration and microclimate regulation. As the ENVI-met model continues to evolve, future studies could benefit from incorporating LAI into the development of tailored individual tree models. This integration would provide additional insights, enhancing the accuracy and reliability of both simulations and ecosystem service quantification efforts.

The overall classification accuracy for tree family classification is 67.1%. Considering the complexity of the urban study sites and the heterogeneity of plausible tree forms and shapes under significant human interference, this result is reasonable, as it falls within the expected accuracy range for multi-class vegetation classification in urban or heterogeneous environments. For example, L. Liu et al. (2017) employed object-based classification using a similar Lidar and hyperspectral dataset, achieving an accuracy of 70.0% at a study site in Vancouver, Canada, comparable to our study area. A review summarizing Lidar-based tree species classification studies reported an average accuracy of 62.2% when six species were classified, with 75% of the studies falling between 59.0% and 66.5% (Michałowska & Rapiński, 2021). The number of families included in the classification significantly influences accuracy. As the number of species or families in a classification attempt increases, the average classification accuracy tends to decrease due to the added complexity and overlap in traits among classes (Voss & Sugumaran, 2008; K. Wang et al., 2018). Misclassifications and gaps in prediction can cause ripple effects in downstream analysis. For example, if a tree from a high-evapotranspiration family is classified into a lower-evapotranspiration family, the resulting simulation may reflect altered microclimate outcomes. Despite such limitations, the overall trends and disparities between the com-

munities remain consistent, supporting our confidence in the validity of the broader workflow.

When it comes to specific families, classification accuracies vary. Betulaceae, Cornaceae, and Fagaceae have relatively low recall rates, likely due to the lack of training samples for these families. Despite oversampling, the model still lacks the ability to capture the variety of possible characteristics of trees from these families, leading to their frequent misclassification into other classes, such as Sapindaceae, which are more dominant within the study scope and are likely to be overfitted by the model. In future studies, collecting additional samples from underrepresented species could enhance classification accuracy. This may include gathering data from areas beyond the immediate scope of the target prediction or modeling work. A more diverse and representative dataset would allow the model to better learn the varied forms and traits of different tree families or species, improving its ability to accurately classify underrepresented classes.

Since this study generalized all tree objects into seven classes, some trees from other rarer families have to be classified into these classes, leading to selection bias. Future studies conducting tree classification for quantitative ecosystem services analysis should pay attention to the classification schemes and purposes. For instance, given that this study's tree classification aimed to support microclimate simulation, there should be more background investigation and adaptation of the classification schemes based on the trees' potential biophysical properties for microclimate regulation. Rosaceae and Cornaceae, being structurally similar as smaller broadleaf deciduous trees, may cause mutual confusion within the classification model, resulting in less accurate distinctions between these two families. For future studies, if some classes are functionally and structurally very similar, researchers can consider merging them into one class without differentiating them since such differentiation would not significantly contribute to the difference in later ecosystem services quantification but introduce more uncertainties and challenges during the classification stage. But there are also tradeoffs and risks when there are too few classes, which limits the ability to test and compare the effects of different kinds of trees belonging to the same general groups (Voss & Sugumaran, 2008; K. Wang et al., 2018).

The DBH prediction and the following size clustering also generated reasonable results. After clustering, we plotted the tree size clustering results for each tree family. Most families have a reasonable distribution of trees of different sizes, such as Sapindaceae, Betulaceae, and Pinaceae, which are trees

with the potential to grow into large sizes. In contrast, Rosaceae and Cornaceae, due to their biological limitations, are rare in the "old" and "very old" sizes. An outlier is Fagaceae, where trees are categorized as either "young" or "very old," lacking trees in the "middle" and "old" sizes. The suggestion would be to add more training samples representing trees from the same family but at different stages of growth.

This study focused on two census tracts, even though the data sources, including Lidar, provide full city coverage. Limiting the analysis to these tracts ensured a manageable scope to test the comparative method. However, expanding the study to include additional sites across the city could enhance reliability and provide a more comprehensive understanding of Portland's urban forest structure. When comparing the two study sites, our analysis provides deeper insights into the density and size distribution of different tree families (trees per area) in different communities, echoing the basic understanding that wealthier communities simply have more trees. Specifically, Site A has nearly twice the density of Sapindaceae trees compared to Site B and also higher densities of Fagaceae and Betulaceae. These large broadleaf deciduous trees are considered more beneficial for microclimate regulation due to their shading and evapotranspiration properties (Armson & Ennos, 2014; Smithers et al., 2018). Conversely, Site B is relatively more abundant in Rosaceae and Cornaceae, which primarily consist of smaller trees that rarely grow into large canopies, limiting their current and future climate regulation benefits (Sanusi et al., 2017). Additionally, some smaller trees in Site A might be obscured under the canopy of larger trees and thus not identified in this study, still outperforming Site B's abundance in the quantity of smaller trees. Site B is more abundant in Pinaceae, which differs from other families as evergreen coniferous in terms of shapes and comparatively lower evapotranspiration rates (Inokoshi et al., 2023). A significant proportion of the Pinaceae trees in Site B appear to have grown naturally and remain largely unmaintained, whereas many Site B's broadleaf deciduous trees are in "young" or "middle" sizes, reflecting the community's limited resources and efforts to actively plant and manage its urban forest in good conditions. This disparity highlights the economic and social challenges faced by the less affluent residents of Site B, and the shorter history of Site B as an evolving residential area transformed and concretized along freeway expansions. In contrast, the wealthier community of Site A, with its more than a century long history as a residential area, has benefited from decades of intentional planting and consistent maintenance of broadleaf deciduous

trees, contributing to a more effective and well-managed urban forest. Consequently, the urban forest composition in Site B is theoretically less favorable for microclimate regulation than Site A's. The classification study not only compares the number of trees between communities, but also examines the detailed composition and quality of urban forests. This provides more comprehensive insights into inequality issues and potential ecosystem service gaps among communities of different backgrounds from various perspectives. Future studies can replicate and expand this approach in other regions and study scopes.

4.2. Integrating remote sensing with microclimate simulation in ENVI-met

A significant contribution of this study is the integration of object-based remote sensing analysis with high-resolution quantitative microclimate simulation. We assigned the target classes so the classification results can fit into the ENVI-met model setup, enabling a quick and reliable setup of the urban forest's physical background model. ENVI-met allows users to create highly detailed models representing reality. The software simulates microclimate conditions under meteorological forcing at spatial and temporal resolutions unattainable by in-situ measurements, as demonstrated and acknowledged in many studies (Crank et al., 2018; Tsoka et al., 2018). However, higher 3D resolution demands exponentially greater computational resources, posing challenges for research and applications with limited resources. In this study, the model is initially set up at a 1-meter spatial resolution to demonstrate its potential, but the resolution is later adjusted to save time and focus on human-centered microclimate parameters, such as elevation that is close to the ground surface. The complete ENVI-met simulation offers high-resolution, quantitative insights into the microclimate conditions within the community.

Tree objects are represented by models from the Albero module in ENVI-met, which has been significantly updated in recent years and includes a preset database of representative species. We chose models from this database, accepting the model and physical parameters set in Albero as reasonable representations of real trees. The model also allows for the creation of new tree models based on known properties such as branching patterns, Leaf Area Index (LAI), and evapotranspiration with its L-String logic and algorithm. We encourage future researchers to use objective, verified knowledge when creating and validating new tree models to represent real trees more accurately and potentially contribute to the Albero database.

The real-case scenarios (Scenario #1) provide the basis for understanding the current situation. Our simulation results indicate that Site A, a more affluent community with a more effective urban forest, would be cooler than Site B, a vulnerable community with a less effective urban forest, during a typical hot summer afternoon. This difference is attributed to variations in urban forest structures, given that other conditions between the two communities are similar and representative of typical American suburban areas, aligning with mainstream studies (Greene et al., 2018; Landry & Chakraborty, 2009; Lehnert et al., 2020). This also establishes a baseline for comparing other proposed scenarios to assess how changes in urban forest characteristics can impact the microclimate's comfort level. Although we did not conduct on-site temperature monitoring to directly validate the ENVI-met model's reliability, which introduces some uncertainty in interpreting the magnitude of predicted cooling effects, its accuracy has been established in previous research through comparisons with in-situ measurements (Eingrüber et al., 2022; Simon et al., 2018). Furthermore, the observed temperature differences between Site A and Site B align with findings from the study that combine ground-based measurements and modeling to produce high-resolution air temperature maps in Portland (Voelkel & Shandas, 2017), which indicates that Site A experiences relatively cooler conditions than Site B. We recognize that, at such fine spatial resolution, empirical validation through conventional means is often infeasible. The purpose of our study is to compare different areas and scenarios, rather than to predict absolute temperature values. Despite the limitation, the observed spatial patterns and relative differences remain robust, such as consistent temperature gradients between tree-covered and non-covered areas, and the cooling advantage of Site A over Site B or among different planting scenarios within a site. However, we encourage future studies to build on our workflow to include supportive validation efforts such as in-situ temperature measurement and calibration of the model.

Our study utilized the object-based microclimate simulation method to create different scenarios. In the sensitivity testing, we investigated the impact of removing all trees (Scenario #2) or just one tree from the study sites (Scenario #3) or changing the varied tree classes to a single tree species (Scenario #4-1, and 4-2). We then compared these simulation results to the original real-case scenarios (Scenario #1). The resulting air-temperature gap highlights the quantitative benefits of tree clusters or individual trees, which is crucial for evaluating total ecosystem services or environmental benefits

(Rahman et al., 2020). Scenario #3, removing one tree, demonstrated that the model is highly sensitive and capable of detecting even slight changes in a single tree. It also confirmed that the model is reliable, producing consistent results in which areas not affected by the removed tree did not experience significant changes in air temperature, as illustrated in Appendix-2.1. Scenarios that switched all trees to either broadleaf deciduous Norway maple (Sapindaceae, Scenario #4-1) or evergreen coniferous pine (Pinaceae, Scenario #4-2) revealed that different tree models significantly impact the microclimate. This is due to the model settings that reflect the actual biophysical properties of different trees. Therefore, it is both feasible and essential to discuss the effects and varying benefits of different types of trees, testing and searching for optimal urban forest compositions that optimize benefits and efficiency, as explored in other studies (Rahman et al., 2020; Richter et al., 2022; Zandler & Samimi, 2024).

Finally, the proposed future scenarios in this study demonstrate how professional urban planners and urban forest specialists can benefit from our workflow. The flexibility of the proposed workflow allows testing of future microclimate conditions to reflect the evolving dynamics of changing urban forests and their environments. Different tree species have varying growth potentials and adapt differently to local environments and changing climates, affecting their future microclimate regulation benefits (McBride & Laćan, 2018). The results of Scenario #5 show that following the current trajectory, the wealthier Site A will gain more benefits from continued growth of existing trees than Site B, widening the existing benefits gap. Future practices can apply more realistic changes, with consideration of different factors such as the species' adaptability to climate change. The scenarios from 6-1 to 6-4 illustrate a proposed situation involving the addition of more trees to Site B. They show that decisions made now may not immediately lead to noticeable differences in impacts, but the benefits will become apparent in the future as the forests evolve. This emphasizes the importance of exercising caution in various aspects of urban forest management.

4.3. Implications and Policy Recommendations

Our simulations indicate that broadleaf deciduous trees, such as those from the Sapindaceae family, are more effective in providing cooling benefits compared to evergreen coniferous trees from the Pinaceae family and smaller deciduous trees from the Rosaceae family. This finding aligns with our hypothesis, leading us to recommend that urban tree planting programs

in Portland communities, such as Site B, prioritize the inclusion of broadleaf deciduous species with the potential to grow to substantial sizes. However, achieving an effective urban forest requires more than just one-time planting; it necessitates consistent and ongoing maintenance to ensure the trees remain healthy and reach maturity. This aspect often presents significant challenges in practice. Our approach offers a valuable tool for urban planning and can be applied in professional practices to test, compare, and support informed decision-making. Urban greening efforts should focus on evaluating and predicting the cost-effectiveness of current actions and their long-term impacts. Given limited resources and attention, sustainable urban forest planning must emphasize precision, scientific rigor, and efficiency to ensure successful outcomes.

This integrated workflow has the potential to be scaled across other areas of Portland or regions with available data, enabling a comprehensive understanding of urban forest conditions and their impacts. In Portland, the existing trained model can be iteratively refined and deployed to other parts of the city. With the ability to automatically set up simulation sites, future studies can easily set up microclimate simulation in other parts of the city, taking advantage of the scalable and efficient tool. It also supports the simulation of improvement proposals tailored to specific community development needs. From a policy and resource management perspective, this approach facilitates scientific evaluation, helping to identify the most cost-effective urban greening strategies. For instance, in Portland, Sapindaceae trees have demonstrated their effectiveness and adaptability but remain unevenly distributed between communities according to our study. Furthermore, the workflow enables the testing of various planting patterns to identify optimal spatial arrangements that maximize ecosystem services, such as determining the best tree placements relative to residential houses. Importantly, this method underscores the critical role of long-term maintenance in urban forestry, highlighting that sustained care and management to ensure trees grow to maturity and maintain good health are as essential as planting them. Achieving this often requires active community engagement to foster an understanding of the value of urban forests and to garner support for maintenance efforts. The City of Portland is actively preparing its 2025 Urban Forest Plan, which aims to establish a comprehensive framework for protecting and expanding the city's urban forests while maximizing their ecosystem services. Our workflow, with its integration of scientific evaluation, scenario testing, and planning adaptability, offers valuable support to this effort, by

providing data-driven insights for sustainable urban forest management that prioritizes equity, efficiency, and resilience.

5. Conclusion

This study presents a comprehensive approach to simulating and quantifying urban forests' microclimate-regulating services, using a case study of two distinct communities in Portland. By integrating high-resolution airborne Lidar data with tree classification and the ENVI-met model, we generated detailed metrics and classifications for individual trees, enabling a comprehensive and efficient urban tree inventory. This method extends beyond traditional pixel-based studies, providing a nuanced understanding of the core suppliers of ecosystem services in urban areas and facilitating explicit object-based microclimate simulations with ENVI-met.

The novelty of this study lies in its integration of Lidar-based individual tree classification with microclimate simulation models that reflect differences between various classes of urban trees. The machine learning tools are effectively applied to a heterogeneous urban area with satisfactory tree family classification accuracy at 67.1% and DBH regression accuracy with R^2 of 0.79, generating an urban tree inventory that can reflect and compare ecosystem services. This approach provides an incentive for other regions to collect and prepare similar datasets. From a microclimate simulation perspective, incorporating Lidar-based machine learning classification data facilitates the possibility of generating larger area tree inventory data for automatic and precise simulation model setup. More studies can thus be conducted on different areas at various scales, making microclimate simulation a more feasible practice.

Applying our methods to two socioeconomically different communities revealed disparities not only in the quantity of urban forests but also in their structure and composition. The wealthier community had a higher density of large broadleaf deciduous trees compared to the more vulnerable community, partially explaining the discrepancies in cooling services, with the average 1.5-meter-above-ground air temperature being 0.23°C (K) different. Alternative scenarios demonstrated how conditions change with removing, replacing, or adding certain trees, providing a meaningful process for urban planning and management professionals to adapt for community environmental investigations.

Future studies can build on this framework by using high-resolution, multi-dimensional remote sensing products to investigate and understand local landscape configurations explicitly in different places. Utilizing this information to simulate and quantify interactions among different environmental features will lead to a holistic understanding of environmental processes and more informed decision-making, enhancing future environmental benefits and climate resilience, and promoting cross-community equity.

Declaration of competing interest

The authors declare that they have no known competing financial interests or personal relationships that could have appeared to influence the work reported in this paper.

Acknowledgments

We gratefully acknowledge Chris Prescott, Shannah Anderson, and their colleagues from the Bureau of Environmental Services, City of Portland, for methodological comments and additional data availability. Special thanks to David L. Miller for editorial suggestions.

During the preparation of this work, the authors used ChatGPT to improve language and readability. After using this tool, the authors reviewed and edited the content as needed and take full responsibility for the content of the publication.

References

Akbari, H., Levinson, R., & Rainer, L. (2005). Monitoring the energy-use effects of cool roofs on California commercial buildings. *Energy and Buildings*, *37*(10), 1007–1016. https://doi.org/10.1016/j.enbuild.2004.11.013

Almeida, C. R. de, Teodoro, A. C., & Gonçalves, A. (2021). Study of the Urban Heat Island (UHI) Using Remote Sensing Data/Techniques: A Systematic Review. *Environments*, *8*(10), Article 10. https://doi.org/10.3390/environments8100105

Alonzo, M., Bookhagen, B., & Roberts, D. A. (2014). Urban tree species mapping using hyperspectral and lidar data fusion. *Remote Sensing of Environment*, *148*, 70–83. https://doi.org/10.1016/j.rse.2014.03.018

Armson, D., & Ennos, R. (2014). A comparison of the growth and cooling effectiveness of five commonly planted urban tree species. *Urban Ecosystems*. https://doi.org/10.1007/s11252-014-0407-7

Aslam, A., & Rana, I. A. (2022). The use of local climate zones in the urban environment: A systematic review of data sources, methods, and themes. *Urban Climate*, *42*, 101120. https://doi.org/10.1016/j.uclim.2022.101120

Beck, H. E., Zimmermann, N. E., McVicar, T. R., Vergopolan, N., Berg, A., & Wood, E. F. (2018). Present and future Köppen-Geiger climate classification maps at 1-km resolution. *Scientific Data*, *5*, 180214. https://doi.org/10.1038/sdata.2018.214

Beucher, S., & Meyer, F. (1993). Segmentation: The Watershed Transformation. Mathematical Morphology in Image Processing. *Optical Engineering*, *34*, 433–481.

Bolund, P., & Hunhammar, S. (1999). Ecosystem services in urban areas. *Ecological Economics*, *29*(2), 293–301. https://doi.org/10.1016/S0921-8009(99)00013-0

Bowler, D. E., Buyung-Ali, L., Knight, T. M., & Pullin, A. S. (2010). Urban greening to cool towns and cities: A systematic review of the empirical evidence. *Landscape and Urban Planning*, *97*(3), 147–155. https://doi.org/10.1016/j.landurbplan.2010.05.006

Bruse, M., & Fleer, H. (1998). Simulating surface–plant–air interactions inside urban environments with a three dimensional numerical model. *Environmental Modelling & Software*, *13*(3), 373–384. https://doi.org/10.1016/S1364-8152(98)00042-5

Buyantuyev, A., & Wu, J. (2010). Urban heat islands and landscape heterogeneity: Linking spatiotemporal variations in surface temperatures to land-cover and socioeconomic patterns. *Landscape Ecology*, *25*(1), 17–33. https://doi.org/10.1007/s10980-009-9402-4

Chakraborty, T., Venter, Z. S., Qian, Y., & Lee, X. (2022). Lower Urban Humidity Moderates Outdoor Heat Stress. *AGU Advances*, *3*(5), e2022AV000729. https://doi.org/10.1029/2022AV000729

Chawla, N. V., Bowyer, K. W., Hall, L. O., & Kegelmeyer, W. P. (2002). SMOTE: Synthetic Minority Over-sampling Technique. *Journal of Artificial Intelligence Research*, *16*, 321–357. https://doi.org/10.1613/jair.953

Chieppa, J., Bush, A., & Mitra, C. (2018). Using "Local Climate Zones" to Detect Urban Heat Island on Two Small Cities in Alabama. *Earth Interactions*. https://doi.org/10.1175/EI-D-17-0020.1

Coops, N. C., Tompalski, P., Goodbody, T. R. H., Queinnec, M., Luther, J. E., Bolton, D. K., White, J. C., Wulder, M. A., van Lier, O. R., & Hermosilla, T. (2021). Modelling lidar-derived estimates of forest attributes over space and time: A review of approaches and future trends. *Remote Sensing of Environ-*

ment, *260*, 112477. https://doi.org/10.1016/j.rse.2021.112477

Crank, P. J., Sailor, D. J., Ban-Weiss, G., & Taleghani, M. (2018). Evaluating the ENVI-met microscale model for suitability in analysis of targeted urban heat mitigation strategies. *Urban Climate*, *26*, 188–197. https://doi.org/10.1016/j.uclim.2018.09.002

Demuzere, M., Kittner, J., Martilli, A., Mills, G., Moede, C., Stewart, I. D., van Vliet, J., & Bechtel, B. (2022). A global map of local climate zones to support earth system modelling and urban-scale environmental science. *Earth System Science Data*, *14*(8), 3835–3873. https://doi.org/10.5194/essd-14-3835-2022

Deng, S., Katoh, M., Yu, X., Hyyppä, J., & Gao, T. (2016). Comparison of Tree Species Classifications at the Individual Tree Level by Combining ALS Data and RGB Images Using Different Algorithms. *Remote Sensing*, *8*(12), Article 12. https://doi.org/10.3390/rs8121034

DiSalvo, A., Fukuda, J., & Ramsey, J. (2017). *Street Tree Inventory Report: City of Portland*. https://www.portland.gov/trees/get-involved/documents/citywide-street-tree-inventory-report/download

Efron, B. (1979). Bootstrap Methods: Another Look at the Jackknife. *The Annals of Statistics*, *7*(1), 1–26. https://doi.org/10.1214/aos/1176344552

Eingrüber, N., Korres, W., & Schneider, K. (2022). Microclimatic field measurements to support microclimatological modelling with ENVI-met for an urban study area in Cologne. *Advances in Science and Research*, *19*, 81–90. https://doi.org/10.5194/asr-19-81-2022

Escobedo, F. J., Giannico, V., Jim, C. Y., Sanesi, G., & Lafortezza, R. (2019). Urban forests, ecosystem services, green infrastructure and nature-based solutions: Nexus or evolving metaphors? *Urban Forestry & Urban Greening*, *37*, 3–12. https://doi.org/10.1016/j.ufug.2018.02.011

Fassnacht, F. E., Latifi, H., Stereńczak, K., Modzelewska, A., Lefsky, M., Waser, L. T., Straub, C., & Ghosh, A. (2016). Review of studies on tree species classification from remotely sensed data. *Remote Sensing of Environment*, *186*, 64–87. https://doi.org/10.1016/j.rse.2016.08.013

Flanagan, B. E., Gregory, E. W., Hallisey, E. J., Heitgerd, J. L., & Lewis, B. (2011). A Social Vulnerability Index for Disaster Management. *Journal of Homeland Security and Emergency Management*, *8*(1). https://doi.org/10.2202/1547-7355.1792

Franklin, J. F., & Dyrness, C. T. (1973). Natural vegetation of Oregon and Washington. *Gen. Tech. Rep. PNW-GTR-008. Portland, OR: U.S. Department of Agriculture, Forest Service, Pacific Northwest Research Station. 427 p, 008.* https://research.fs.usda.gov/treesearch/26203

Gašparović, M., Dobrinić, D., & Pilaš, I. (2023). Mapping of Allergenic Tree Species in Highly Urbanized Area Using PlanetScope Imagery—A Case Study of Zagreb, Croatia. *Forests*, *14*(6), Article 6. https://doi.org/10.3390/f14061193

Gottesman, R., & Shierman, E. (2019). Has Portland been Demolishing its Green Spaces? A Remote Sensing Analysis of Portland's Urban Vegetation. *The Hatfield Graduate Journal of Public Affairs*, *3*(2). https://doi.org/10.15760/hgjpa.2019.3.2.5

Greene, C. S., Robinson, P. J., & Millward, A. A. (2018). Canopy of advantage: Who benefits most from city trees? *Journal of Environmental Management*, *208*, 24–35. https://doi.org/10.1016/j.jenvman.2017.12.015

Grimmond, S. (2007). Urbanization and global environmental change: Local effects of urban warming. *The Geographical Journal*, *173*(1), 83–88. https://doi.org/10.1111/j.1475-4959.2007.232_3.x

Hancock, S., Anderson, K., Disney, M., & Gaston, K. J. (2017). Measurement of fine-spatial-resolution 3D vegetation structure with airborne waveform lidar: Calibration and validation with voxelised terrestrial lidar. *Remote Sensing of Environment*, *188*, 37–50. https://doi.org/10.1016/j.rse.2016.10.041

Hathway, E. A., & Sharples, S. (2012). The interaction of rivers and urban form in mitigating the Urban Heat Island effect: A UK case study. *Building and Environment*, *58*, 14–22. https://doi.org/10.1016/j.buildenv.2012.06.013

Hazell, B. (2020). *2019 Metro Lidar Project*. GeoTerra, Inc.

Hoffman, J. S., Shandas, V., & Pendleton, N. (2020). The Effects of Historical Housing Policies on Resident Exposure to Intra-Urban Heat: A Study of 108 US Urban Areas. *Climate*, *8*(1), Article 1. https://doi.org/10.3390/cli8010012

Inokoshi, S., Gomi, T., Chiu, C.-W., Onda, Y., Hashimoto, A., Zhang, Y., & Saitoh, T. M. (2023). A watershed-scale evapotranspiration model considering forest type, stand parameters, and climate factors. *Forest Ecology and Management*, *547*, 121387. https://doi.org/10.1016/j.foreco.2023.121387

Isenburg, M. (2012). *LAStools—Efficient LiDAR processing software* (Version 230212) [Computer software]. rapidlasso GmbH. https://rapidlasso.com/lastools/

Jakubowski, M. K., Li, W., Guo, Q., & Kelly, M. (2013). Delineating Individual Trees from Lidar Data: A Comparison of Vector- and Raster-based Segmentation Approaches. *Remote Sensing*, *5*(9), Article 9. https://doi.org/10.3390/rs5094163

Jänicke, B., Milošević, D., & Manavvi, S. (2021). Review of User-Friendly Models to Improve the Urban Micro-Climate. *Atmosphere*, *12*(10), 1291. https://doi.org/10.3390/atmos12101291

Jenerette, G. D., Harlan, S. L., Stefanov, W. L., & Martin, C. A. (2011). Ecosystem services and urban heat riskscape moderation: Water, green spaces, and social inequality in Phoenix, USA. *Ecological Applications*, *21*(7), 2637–2651.

Jesdale, B. M., Morello-Frosch, R., & Cushing, L. (2013). The Racial/Ethnic Distribution of Heat Risk–Related Land Cover in Relation to Residential Segregation. *Environmental Health Perspectives*, *121*(7), 811–817. https://doi.org/10.1289/ehp.1205919

Jiang, S., Huang, F., Zhan, W., Bechtel, B., Liu, Z., Demuzere, M., Huang, Y., Xu, Y., Quan, J., Xia, W., Ma, L., Hong, F., Jiang, L., Lai, J., Wang, C., Kong, F., Du, H., Miao, S., Chen, Y., & Zhang, X. (2021). *Mapping Local Climate Zones: A Bibliometric Meta-Analysis and Systematic Review*. OSF Preprints. https://doi.org/10.31219/osf.io/c2bez

Kim, J., Khouakhi, A., Corstanje, R., & Johnston, A. S. A. (2024). Greater local cooling effects of trees across globally distributed urban green spaces. *Science of The Total Environment*, *911*, 168494. https://doi.org/10.1016/j.scitotenv.2023.168494

Kim, S., Hinckley, T., & Briggs, D. (2011). Classifying individual tree genera using stepwise cluster analysis based on height and intensity metrics derived from airborne laser scanner data. *Remote Sensing of Environment*, *115*(12), 3329–3342. https://doi.org/10.1016/j.rse.2011.07.016

Klobucar, B., Sang, N., & Randrup, T. B. (2021). Comparing ground and remotely sensed measurements of urban tree canopy in private residential property. *Trees, Forests and People*, *5*, 100114. https://doi.org/10.1016/j.tfp.2021.100114

Konarska, J., Uddling, J., Holmer, B., Lutz, M., Lindberg, F., Pleijel, H., & Thorsson, S. (2016). Transpiration of urban trees and its cooling effect in a high latitude city. *International Journal of Biometeorology*, *60*(1), 159–172. https://doi.org/10.1007/s00484-015-1014-x

Kong, F., Yin, H., Wang, C., Cavan, G., & James, P. (2014). A satellite image-based analysis of factors contributing to the green-space cool island intensity on a city scale. *Urban Forestry & Urban Greening*, *13*(4), 846–853. https://doi.org/10.1016/j.ufug.2014.09.009

Landry, S. M., & Chakraborty, J. (2009). Street Trees and Equity: Evaluating the Spatial Distribution of an Urban Amenity. *Environment and Planning A: Economy and Space*, *41*(11), 2651–2670. https://doi.org/10.1068/a41236

Lehnert, E. A., Wilt, G., Flanagan, B., & Hallisey, E. (2020). Spatial exploration of the CDC's Social Vulnerability Index and heat-related health outcomes in Georgia. *International Journal of Disaster Risk Reduction*, *46*, 101517. https://doi.org/10.1016/j.ijdrr.2020.101517

Lindberg, F., Holmer, B., & Thorsson, S. (2008). SOLWEIG 1.0 – Modelling spatial variations of 3D radiant fluxes and mean radiant temperature in complex urban settings. *International Journal of Biometeorology*, *52*(7), 697–713. https://doi.org/10.1007/s00484-008-0162-7

Liu, L., Coops, N. C., Aven, N. W., & Pang, Y. (2017). Mapping urban tree species using integrated airborne hyperspectral and LiDAR remote sensing data. *Remote Sensing of Environment*, *200*, 170–182. https://doi.org/10.1016/j.rse.2017.08.010

Liu, Z., Cheng, W., Jim, C. Y., Morakinyo, T. E., Shi, Y., & Ng, E. (2021). Heat mitigation benefits of urban green and blue infrastructures: A systematic review of modeling techniques, validation and scenario simulation in ENVI-met V4. *Building and Environment*, *200*, 107939. https://doi.org/10.1016/j.buildenv.2021.107939

Liu, Z., Zheng, S., & Zhao, L. (2018). Evaluation of the ENVI-Met Vegetation Model of Four Common Tree Species in a Subtropical Hot-Humid Area. *Atmosphere*, *9*(5), Article 5. https://doi.org/10.3390/atmos9050198

Livesley, S. J., McPherson, E. G., & Calfapietra, C. (2016). The Urban Forest and Ecosystem Services: Impacts on Urban Water, Heat, and Pollution Cycles at the Tree, Street, and City Scale. *Journal of Environmental Quality*, *45*(1), 119–124. https://doi.org/10.2134/jeq2015.11.0567

Makido, Y., Hellman, D., & Shandas, V. (2019). Nature-Based Designs to Mitigate Urban Heat: The Efficacy of Green Infrastructure Treatments in Portland, Oregon. *Atmosphere*, *10*(5), 282. https://doi.org/10.3390/atmos10050282

Maronga, B., Gryschka, M., Heinze, R., Hoffmann, F., Kanani-Sühring, F., Keck, M., Ketelsen, K., Letzel, M. O., Sühring, M., & Raasch, S. (2015). The Parallelized Large-Eddy Simulation Model (PALM) version 4.0 for atmospheric and oceanic flows: Model formulation, recent developments, and future perspectives. *Geoscientific Model Development*, *8*(8), 2515–2551. https://doi.org/10.5194/gmd-8-2515-2015

McBride, J. R., & Laćan, I. (2018). The impact of climate-change induced temperature increases on the suitability of street tree species in California (USA) cities. *Urban Forestry & Urban Greening*, *34*, 348–356. https://doi.org/10.1016/j.ufug.2018.07.020

McPherson, E. G., Simpson, J. R., Xiao, Q., & Wu, C. (2011). Million trees Los Angeles canopy cover and benefit assessment. *Landscape and Urban Planning*, *99*(1), 40–50. https://doi.org/10.1016/j.landurbplan.2010.08.011

McPherson, E. G., van Doorn, N., & de Goede, J. (2016). Structure, function and value of street trees in California, USA. *Urban Forestry & Urban Greening*, *17*,

104–115. https://doi.org/10.1016/j.ufug.2016.03.013

McRae, I., Freedman, F., Rivera, A., Li, X., Dou, J., Cruz, I., Ren, C., Dronova, I., Fraker, H., & Bornstein, R. (2020). Integration of the WUDAPT, WRF, and ENVI-met models to simulate extreme daytime temperature mitigation strategies in San Jose, California. *Building and Environment*, *184*, 107180. https://doi.org/10.1016/j.buildenv.2020.107180

McRae, I. K. (2017). *Bridging Scientific Research Into The Applied Realm: A case study of the Urban Heat Island effect in Oakland, California*. University of California, Berkeley.

Metro Data Resource Center. (2022, June 22). *Canopy 2019*. https://rlisdiscovery.oregonmetro.gov/datase 2019/about

Michałowska, M., & Rapiński, J. (2021). A Review of Tree Species Classification Based on Airborne LiDAR Data and Applied Classifiers. *Remote Sensing*, *13*(3), Article 3. https://doi.org/10.3390/rs13030353

Münzinger, M., Prechtel, N., & Behnisch, M. (2022). Mapping the urban forest in detail: From LiDAR point clouds to 3D tree models. *Urban Forestry & Urban Greening*, *74*, 127637. https://doi.org/10.1016/j.ufug.2022.127637

Naserikia, M., Hart, M. A., Nazarian, N., Bechtel, B., Lipson, M., & Nice, K. A. (2023). Land surface and air temperature dynamics: The role of urban form and seasonality. *Science of The Total Environment*, *905*, 167306. https://doi.org/10.1016/j.scitotenv.2023.167306

Nesbitt, L., & Meitner, M. (2016). Exploring Relationships between Socioeconomic Background and Urban Greenery in Portland, OR. *Forests*, *7*(12), 162. https://doi.org/10.3390/f7080162

Nguyen, V. D., Roman, L. A., Locke, D. H., Mincey, S. K., Sanders, J. R., Smith Fichman, E., Duran-Mitchell, M., & Tobing, S. L. (2017). Branching out to residential lands: Missions and strategies of five tree distribution programs in the U.S. *Urban Forestry & Urban Greening*, *22*, 24–35. https://doi.org/10.1016/j.ufug.2017.01.007

NOAA. (2021, May). *U.S. Climate Normals*. National Centers for Environmental Information (NCEI). https://www.ncei.noaa.gov/products/land-based-station/us-climate-normals

Nowak, D. J., & Dwyer, J. F. (2007). Understanding the Benefits and Costs of Urban Forest Ecosystems. In J. E. Kuser (Ed.), *Urban and Community Forestry in the Northeast* (pp. 25–46). Springer Netherlands. https://doi.org/10.1007/978-1-4020-4289-8_2

Ozkeresteci, I., Crewe, K., Brazel, A. J., & Bruse, M. (2003). *Use and Evaluation of the ENVI-MET Model for Environmental Design and Planning: An*

Experiment on Linear Parks. https://www.semanticscholar.org/paper/USE-AND-EVALUATION-OF-THE-ENVI-MET-MODEL-FOR-DESIGN-Parks.-Ozkeresteci/b74e913b1d0b54269ed5e661238b428c1ad671e2

Pedregosa, F., Varoquaux, G., Gramfort, A., Michel, V., Thirion, B., Grisel, O., Blondel, M., Prettenhofer, P., Weiss, R., Dubourg, V., Vanderplas, J., Passos, A., Cournapeau, D., Brucher, M., Perrot, M., & Duchesnay, É. (2011). Scikit-learn: Machine Learning in Python. *Journal of Machine Learning Research*, *12*(85), 2825–2830.

Plowright, A., & Roussel, J.-R. (2021). *ForestTools: Analyzing Remotely Sensed Forest Data* (Version 0.2.5) [Computer software]. https://CRAN.R-project.org/package=ForestTools

Popescu, S. C., & Wynne, R. H. (2004). Seeing the Trees in the Forest. *Photogrammetric Engineering & Remote Sensing*, *70*(5), 589–604. https://doi.org/10.14358/PERS.70.5.589

Portland Parks & Recreation. (2021, January). *Park Tree Inventory Report*. ArcGIS StoryMaps. https://storymaps.arcgis.com/stories/b37a095013304e2a93639b29b342c35c

Rahman, M. A., Stratopoulos, L. M. F., Moser-Reischl, A., Zölch, T., Häberle, K.-H., Rötzer, T., Pretzsch, H., & Pauleit, S. (2020). Traits of trees for cooling urban heat islands: A meta-analysis. *Building and Environment*, *170*, 106606. https://doi.org/10.1016/j.buildenv.2019.106606

Richter, R., Ballasus, H., Engelmann, R. A., Zielhofer, C., Sanaei, A., & Wirth, C. (2022). Tree species matter for forest microclimate regulation during the drought year 2018: Disentangling environmental drivers and biotic drivers. *Scientific Reports*, *12*(1), 17559. https://doi.org/10.1038/s41598-022-22582-6

Roberts, D. A., Dennison, P. E., Roth, K. L., Dudley, K., & Hulley, G. (2015). Relationships between dominant plant species, fractional cover and Land Surface Temperature in a Mediterranean ecosystem. *Remote Sensing of Environment*, *167*, 152–167. https://doi.org/10.1016/j.rse.2015.01.026

Roman, L. A., Pearsall, H., Eisenman, T. S., Conway, T. M., Fahey, R. T., Landry, S., Vogt, J., van Doorn, N. S., Grove, J. M., Locke, D. H., Bardekjian, A. C., Battles, J. J., Cadenasso, M. L., van den Bosch, C. C. K., Avolio, M., Berland, A., Jenerette, G. D., Mincey, S. K., Pataki, D. E., & Staudhammer, C. (2018). Human and biophysical legacies shape contemporary urban forests: A literature synthesis. *Urban Forestry & Urban Greening*, *31*, 157–168. https://doi.org/10.1016/j.ufug.2018.03.004

Sanusi, R., Johnstone, D., May, P., & Livesley, S. J. (2017). Microclimate benefits that different street tree species provide to sidewalk pedestrians relate to differences in Plant Area Index. *Landscape and Urban Planning*, *157*, 502–511.

https://doi.org/10.1016/j.landurbplan.2016.08.010

Schwarz, K., Fragkias, M., Boone, C. G., Zhou, W., McHale, M., Grove, J. M., O'Neil-Dunne, J., McFadden, J. P., Buckley, G. L., Childers, D., Ogden, L., Pincetl, S., Pataki, D., Whitmer, A., & Cadenasso, M. L. (2015). Trees Grow on Money: Urban Tree Canopy Cover and Environmental Justice. *PLoS ONE*, *10*(4), e0122051. https://doi.org/10.1371/journal.pone.0122051

Shahtahmassebi, A. R., Li, C., Fan, Y., Wu, Y., lin, Y., Gan, M., Wang, K., Malik, A., & Blackburn, G. A. (2021). Remote sensing of urban green spaces: A review. *Urban Forestry & Urban Greening*, *57*, 126946. https://doi.org/10.1016/j.ufug.2020.126946

Shandas, V., Voelkel, J., Williams, J., & Hoffman, J. (2019). Integrating Satellite and Ground Measurements for Predicting Locations of Extreme Urban Heat. *Climate*, *7*(1), Article 1. https://doi.org/10.3390/cli7010005

Simon, H., Lindén, J., Hoffmann, D., Braun, P., Bruse, M., & Esper, J. (2018). Modeling transpiration and leaf temperature of urban trees – A case study evaluating the microclimate model ENVI-met against measurement data. *Landscape and Urban Planning*, *174*, 33–40. https://doi.org/10.1016/j.landurbplan.2018.03.003

Simon, H., Sinsel, T., & Bruse, M. (2020). Introduction of Fractal-Based Tree Digitalization and Accurate In-Canopy Radiation Transfer Modelling to the Microclimate Model ENVI-met. *Forests*, *11*(8), Article 8. https://doi.org/10.3390/f11080869

Smithers, R. J., Doick, K. J., Burton, A., Sibille, R., Steinbach, D., Harris, R., Groves, L., & Blicharska, M. (2018). Comparing the relative abilities of tree species to cool the urban environment. *Urban Ecosystems*, *21*(5), 851–862. https://doi.org/10.1007/s11252-018-0761-y

Steenberg, J. W. N., Millward, A. A., Nowak, D. J., Robinson, P. J., & Ellis, A. (2017). Forecasting Urban Forest Ecosystem Structure, Function, and Vulnerability. *Environmental Management*, *59*(3), 373–392. https://doi.org/10.1007/s00267-016-0782-3

Stewart, I. D., & Oke, T. R. (2012). Local Climate Zones for Urban Temperature Studies. *Bulletin of the American Meteorological Society*, *93*(12), 1879–1900. https://doi.org/10.1175/BAMS-D-11-00019.1

Stone, M. (1974). Cross-Validatory Choice and Assessment of Statistical Predictions. *Journal of the Royal Statistical Society. Series B (Methodological)*, *36*(2), 111–147.

Tian, L., Qu, Y., & Qi, J. (2021). Estimation of Forest LAI Using Discrete Airborne LiDAR: A Review. *Remote Sensing*, *13*(12), Article 12.

https://doi.org/10.3390/rs13122408

Tsoka, S., Tsikaloudaki, A., & Theodosiou, T. (2018). Analyzing the ENVI-met microclimate model's performance and assessing cool materials and urban vegetation applications–A review. *Sustainable Cities and Society*, *43*, 55–76. https://doi.org/10.1016/j.scs.2018.08.009

Voelkel, J., & Shandas, V. (2017). Towards Systematic Prediction of Urban Heat Islands: Grounding Measurements, Assessing Modeling Techniques. *Climate*, *5*(2), Article 2. https://doi.org/10.3390/cli5020041

Voss, M., & Sugumaran, R. (2008). Seasonal Effect on Tree Species Classification in an Urban Environment Using Hyperspectral Data, LiDAR, and an Object- Oriented Approach. *Sensors*, *8*(5), Article 5. https://doi.org/10.3390/s8053020

Wang, C., Ren, Z., Chang, X., Wang, G., Hong, X., Dong, Y., Guo, Y., Zhang, P., Ma, Z., & Wang, W. (2023). Understanding the cooling capacity and its potential drivers in urban forests at the single tree and cluster scales. *Sustainable Cities and Society*, *93*, 104531. https://doi.org/10.1016/j.scs.2023.104531

Wang, K., Wang, T., & Liu, X. (2018). A Review: Individual Tree Species Classification Using Integrated Airborne LiDAR and Optical Imagery with a Focus on the Urban Environment. *Forests*, *10*(1), 1. https://doi.org/10.3390/f10010001

Weng, Q. H., Lu, D. S., & Schubring, J. (2004). Estimation of land surface temperature-vegetation abundance relationship for urban heat island studies. *Remote Sensing of Environment*, *89*(4), 467–483. https://doi.org/10.1016/j.rse.2003.11.005

Wolf, K. L., Lam, S. T., McKeen, J. K., Richardson, G. R. A., van den Bosch, M., & Bardekjian, A. C. (2020). Urban Trees and Human Health: A Scoping Review. *International Journal of Environmental Research and Public Health*, *17*(12), 4371. https://doi.org/10.3390/ijerph17124371

Yao, X., & Kim, M. (2023). From Local to Micro: Exploratory Data Analysis on Urban Forests and Microclimates in Portland, Oregon, USA. *IGARSS 2023 - 2023 IEEE International Geoscience and Remote Sensing Symposium*, 2095–2098. https://doi.org/10.1109/IGARSS52108.2023.10282088

Yao, X., & Kim, M. (2024). A Lidar-based Method for 3D Urban Forest Evaluation and Microclimate Assessment, a Case Study in Portland, Oregon, USA. *Authorea Preprints*. https://essopenarchive.org/doi/full/10.22541/essoar.170914530.09781933

Yu, X., Hyyppä, J., Vastaranta, M., Holopainen, M., & Viitala, R. (2011). Predicting individual tree attributes from airborne laser point clouds based on the random forests technique. *ISPRS Journal of Photogrammetry and Remote Sensing*, *66*(1), 28–37. https://doi.org/10.1016/j.isprsjprs.2010.08.003

Yuan, F., & Bauer, M. E. (2007). Comparison of impervious surface area and normalized difference vegetation index as indicators of surface urban heat island effects in Landsat imagery. *Remote Sensing of Environment*, *106*(3), 375–386. https://doi.org/10.1016/j.rse.2006.09.003

Zandler, H., & Samimi, C. (2024). Cooling Potential of Urban Tree Species during Extreme Heat and Drought: A Thermal Remote Sensing Assessment. *Remote Sensing*, *16*(12), Article 12. https://doi.org/10.3390/rs16122059

Zhang, C., Zhou, Y., & Qiu, F. (2015). Individual Tree Segmentation from LiDAR Point Clouds for Urban Forest Inventory. *Remote Sensing*, *7*(6), Article 6. https://doi.org/10.3390/rs70607892

Zhang, Z., Kazakova, A., Moskal, L. M., & Styers, D. M. (2016). Object-Based Tree Species Classification in Urban Ecosystems Using LiDAR and Hyperspectral Data. *Forests*, *7*(6), Article 6. https://doi.org/10.3390/f7060122

Zhao, C., & Sander, H. A. (2018). Assessing the sensitivity of urban ecosystem service maps to input spatial data resolution and method choice. *Landscape and Urban Planning*, *175*, 11–22. https://doi.org/10.1016/j.landurbplan.2018.03.007

Zhou, D., Xiao, J., Bonafoni, S., Berger, C., Deilami, K., Zhou, Y., Frolking, S., Yao, R., Qiao, Z., & Sobrino, J. A. (2019). Satellite Remote Sensing of Surface Urban Heat Islands: Progress, Challenges, and Perspectives. *Remote Sensing*, *11*(1), Article 1. https://doi.org/10.3390/rs11010048

Zhu, X., Skidmore, A. K., Wang, T., Liu, J., Darvishzadeh, R., Shi, Y., Premier, J., & Heurich, M. (2018). Improving leaf area index (LAI) estimation by correcting for clumping and woody effects using terrestrial laser scanning. *Agricultural and Forest Meteorology*, *263*, 276–286. https://doi.org/10.1016/j.agrformet.2018.08.026

Appendices

1. List of metrics for the metrics used for individual tree analysis. All metrics are used for all the tree family classification, DBH prediction and tree size clustering, with the importance score for Random Forest supported tree family classification listed for reference of the importance.

	Metric name	Notes	Importance score for Random Forest family classification
1	all	Total number of points	0.0134

	Metric name	Notes	Importance score for Random Forest family classification
2	min	Min height above the cutoff (1.37 m)	0.0139
3	max	Max height above the cutoff (1.37 m)	0.0120
4	avg	Average height above the cutoff (1.37 m)	0.0213
5	qav	Average square height (1.37 m)	0.0178
6	std	Standard deviation	0.0213
7	ske	Skewness	0.0238
8	kur	Kurtosis	0.0142
9	hom	Height & intensity metric known as "Height of Median Energy"	0.0106
10	p10	"Percentile": Height percentiles	0.0127
11	p25		0.0158
12	p50		0.0185
13	p75		0.0139
14	p90		0.0184
15	b10	"Bincentile": percentage or fraction of points between the height cutoff (aka breast height) and the maximum height	0.0148
16	b20		0.0132
17	b30		0.0153
18	b40		0.0137
19	b50		0.0124
20	b60		0.0115
21	b70		0.0101
22	b80		0.0115
23	b90		0.0128

	Metric name	Notes	Importance score for Random Forest family classification
24	d00 (0-2m)	Height raster [0-2,2-5,5-8] in which the counts are divided by the total number of points and scaled to a percentage	0.0114
25	d01 (2-5m)		0.0191
26	d02 (5-8m)		0.0103
27	cov_gap	The inverse of the canopy cover (100% - canopy)	0.0195
28	dns_gap	The inverse of the density, the canopy density as the number of all points above the cover cutoff divided by the number of all returns	0.0195
29	Height	The Height of the highest point, from ForestTools with nDSM	0.0294
30	crownArea	Crown area, from ForestTools with nDSM	0.0263
31	SArea	Surface area, from ForestTools with nDSM	0.0183
32	Min_Slope	Min slope of the surface, from ForestTools with nDSM	0.0311
33	Max_Slope	Max slope of the surface, from ForestTools with nDSM	0.0135
34	Avg_Slope	Avg slope of the surface, from ForestTools with nDSM	0.0074
35	Z_Mean_FirstReturn	Mean height of the first returns	0.0308
36	2018_R	2018 OSIP R band	0.0175
37	2018_G	2018 OSIP G band	0.0181
38	2018_B	2018 OSIP B band	0.0162
39	2018_N	2018 OSIP NIR band	0.0194

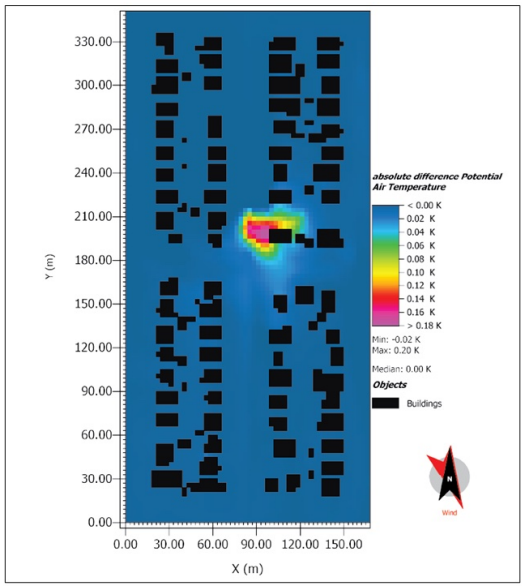
	Metric name	Notes	Importance score for Random Forest family classification
40	2020_R	2020 NAIP R band	0.0177
41	2020_G	2020 NAIP G band	0.0214
42	2020_B	2020 NAIP B band	0.0177
43	2020_N	2020 NAIP NIR band	0.0233
44	averageNDVI	Mean NDVI from 2018 OSIP and 2020 NAIP	0.0331
45	1re	Count of 1st return	0.0252
46	2re	Count of 2nd return	0.0113
47	3re	Count of 3rd return	0.0206
48	4re	Count of 4th return	0.0217
49	FirstofManyre	Count of first of many return	0.0140
50	LastofManyre	Count of last of many return	0.0367
51	Lastre	Count of last return	0.0217
52	NonFirstoverFirst	Count of non-first return over first return	0.0148

2. ENVI-met microclimate simulation results:

    1. Scenario 3 (Sensitivity Tests): Single Tree Removal

Description: This scenario involves the removal of Sample Tree X to evaluate the microclimate impact of a single tree at Site A.

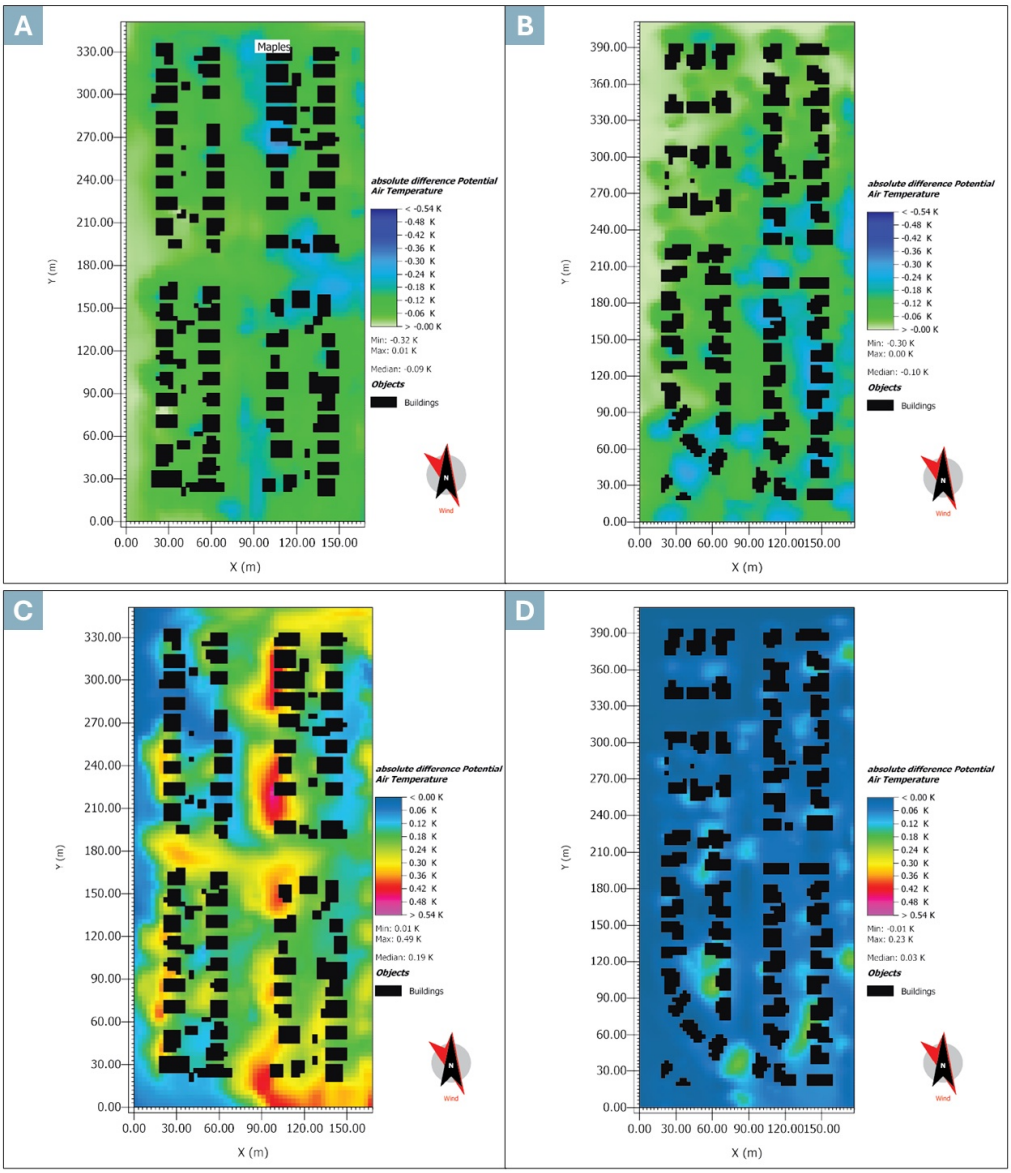
Figure: Temperature difference maps comparing the scenario with and without the tree X, illustrating its quantitative effect on the microclimate. Temperature units: Kelvin (K) or Degree Celsius (°C)



2. Scenario 4 (Sensitivity Tests): Species Substitution

Description: This scenario tests the impact of replacing all trees with either maple or pine species, without altering tree sizes. Switching to maple generally reduces temperatures, while switching to pine increases temperatures.

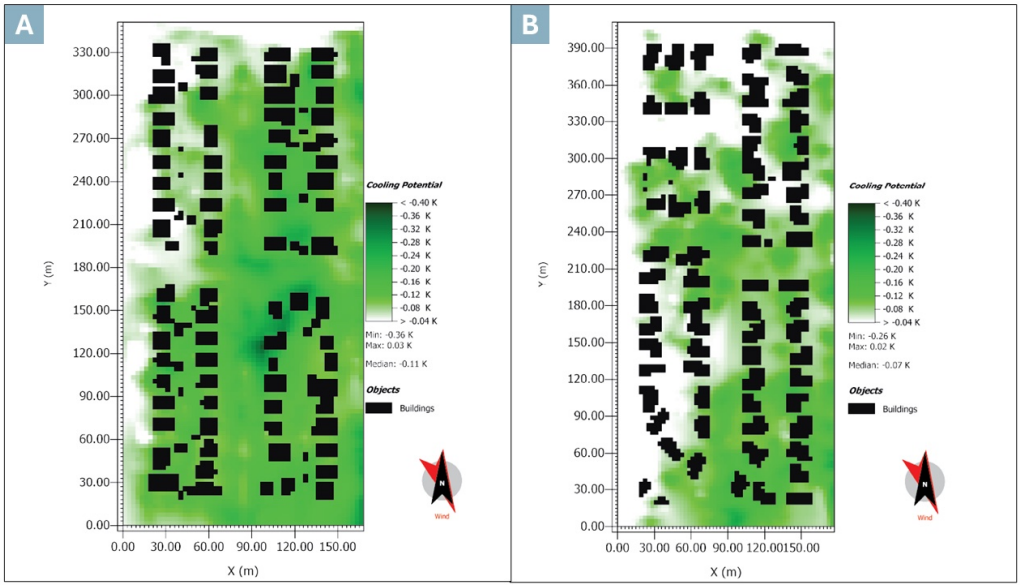
Figures: Temperature difference maps compared to the real case scenarios are provided for each site and species substitution. A: Site A with all trees switched to maple. B: Site B with all trees switched to maple. C: Site A with all trees switched to pine. D: Site B with all trees switched to pine. Temperature units: Kelvin (K) or Degree Celsius (°C)



3. Scenario 5 (Alternative Planning): Future Tree Growth

Description: This scenario examines the future microclimate impact as trees grow to their mature sizes. For Sapindaceae, Pinaceae, Fagaceae, and Betulaceae: "young" and "middle" trees grow to "old," and "old" trees grow to "very old." For Rosaceae and Cornaceae: "young" trees grow to "middle".

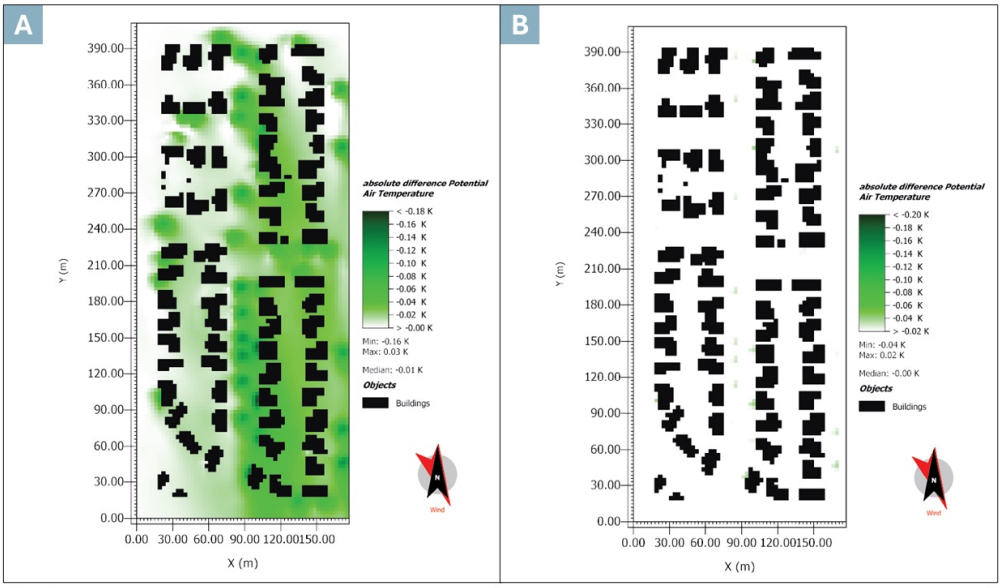
Figures: Temperature difference maps compared to the real case scenarios are provided for each site and species substitution. A: Temperature difference at Site A after tree growth. B: Temperature difference at Site B after tree growth. Temperature units: Kelvin (K) or Degree Celsius (°C)



4. Scenario 6 (Alternative Planning): Planting 40 Trees

Description: This scenario assesses the impact of adding 40 new trees of different species (maples and cherries) and sizes (young for both species, middle for cherry, and old for maple) to Site B. Future sizes (old for maple and middle for cherry) are determined based on the potential of the species.

Figures: Temperature difference maps compared to the real case scenarios are provided for each site and species substitution. A: Adding 40 young maples. B: Adding 40 young cherries. C: 40 maples grow to ”old” sizes. D: 40 cherries grow to ”middle” sizes. Temperature units: Kelvin (K) or Degree Celsius (°C)


A
B
C
D
Y (m)
X (m)
0.00 30.00 60.00 90.00 120.00 150.00
0.00 30.00 60.00 90.00 120.00 150.00 180.00 210.00 240.00 270.00 300.00 330.00 360.00 390.00
absolute difference Potential Air Temperature
< -0.18 K
-0.16 K
-0.14 K
-0.12 K
-0.10 K
-0.08 K
-0.06 K
-0.04 K
-0.02 K
> -0.00 K
Min: -0.16 K
Max: 0.03 K
Median: -0.01 K
Objects
Buildings
absolute difference Potential Air Temperature
< -0.20 K
-0.18 K
-0.16 K
-0.14 K
-0.12 K
-0.10 K
-0.08 K
-0.06 K
-0.04 K
> -0.02 K
Min: -0.04 K
Max: 0.02 K
Median: -0.00 K
Objects
Buildings
Cooling Potential
< -0.40 K
-0.36 K
-0.32 K
-0.28 K
-0.24 K
-0.20 K
-0.16 K
-0.12 K
-0.08 K
> -0.04 K
Min: -0.37 K
Max: 0.00 K
Median: -0.08 K
Objects
Buildings
Cooling Potential
< -0.40 K
-0.36 K
-0.32 K
-0.28 K
-0.24 K
-0.20 K
-0.16 K
-0.12 K
-0.08 K
> -0.04 K
Min: -0.16 K
Max: 0.03 K
Median: -0.02 K
Objects
Buildings